Habitat adaptation determines dark septate endophyte mediated stabilization of the soil-root-plant continuum under sulfate salinity

Yinli Bi

ylbi88@126.com

China University of Mining and Technology (Beijing) https://orcid.org/0000-0002-5562-1045

Shishuang Zhang
Jianying Zhang
Yuguang Zhang
Hai Tan
Jiapeng Kang

Research Article

Keywords: Dark septate endophytes, Suaeda salsa, Salt tolerance, Pyrimidine metabolism, Rhizosphere, Ion homeostasis

Posted Date: August 12th, 2026

DOI: https://doi.org/10.21203/rs.3.rs-10377623/v1

Abstract

Background Global soil salinization is intensifying, yet the mechanisms determining whether beneficial plant–microbe symbioses remain functional under extreme ionic stress remain poorly understood.

Methods Using the halophyte *Suaeda salsa* and two ecologically distinct dark septate endophytes (DSEs), we evaluated symbiotic performance across a Na_2SO_4 gradient (0-0.4 M) by integrating physiological, ionomic, rhizosphere, and untargeted metabolomic analyses. Symbiotic outcomes were strongly dependent on fungal habitat adaptation.

Results The halophytic isolate *Alternaria chlamydospora* SC11 maintained stable colonization and consistently enhanced plant survival and growth under increasing salinity, whereas the non-adapted isolate As17463 progressively lost functionality. SC11 sustained K, N, and P homeostasis despite high Na^+ accumulation, preserved root structural integrity and rhizosphere enzymatic activity, and promoted persistent activation of pyrimidine and nucleotide-sugar metabolism. Integrative analyses revealed strong coupling between rhizosphere properties and host metabolic responses, indicating coordinated regulation across the soil-root-plant continuum.

Conclusion Persistent colonization by habitat-adapted DSEs strengthens the osmoregulatory capacity, nutrient homeostasis, and functional stability of *S. salsa* under severe sulfate salinity. This study provides mechanistic criteria for selecting effective fungal inoculants and offers theoretical guidance and practical support for microbial-assisted restoration and sustainable management of saline-alkali environments.

Introduction

Soil salinization is a critical global constraint on ecosystem functioning and agricultural productivity (Wang et al., 2025a). Nearly one billion hectares of land worldwide are affected by salinity, and this area is projected to expand substantially by 2050, driven by climate variability, intensifying food demand, and unsustainable land-use practices (Ivushkin et al., 2019; Negacz et al., 2021). Excessive salt accumulation profoundly alters soil physicochemical properties, resulting in organic matter depletion, reduced water-holding capacity, impaired soil permeability, and compromised aggregate stability (Bello et al., 2021). These impacts are particularly severe in coastal, arid, and semi-arid regions (Saddhe et al., 2020). At the plant level, elevated salinity caused oxidative damage and Na^+/K^+ imbalance, thereby impairing hormonal regulation, nutrient acquisition, root development, and DNA replication (Kaya et al., 2024; Sun et al., 2015), while also triggering specific metabolic rearrangements tied to sulfur assimilation (De Castro et al., 2018). These combined effects ultimately exacerbated growth inhibition and frequently resulted in plant death, although targeted mitigation strategies could effectively restore physiological homeostasis(Kaya et al., 2024). Salinized soils are typically characterized by increased pH, elevated sodium adsorption ratio (SAR) and exchangeable sodium percentage (ESP), and diminished cation

exchange capacity (CEC), collectively suppressing soil functionality and microbial diversity (Abhayawickrama et al., 2020).

In response, plant-associated endophytic fungi have emerged as promising ecological tools sustainable saline land management (Fracetto et al., 2023). This perspective is reinforced by recent work on saline-alkali soil remediation, which further indicates that microbial community assembly and functional differentiation underpin restoration success (Wang et al., 2025b), underscoring the critical need to pinpoint microbial traits that retain functionality under severe salinity. Dark septate endophytes (DSEs), a phylogenetically diverse group of root-colonizing ascomycetes (Grünig et al., 2011; Knapp et al., 2015; Rodriguez et al., 2009), are particularly notable due to their broad host range and frequent occurrence in saline habitats (Zhang et al., 2025). DSEs enhance host performance by facilitating nutrient acquisition (Tan et al., 2025; Usuki and Narisawa, 2007), strengthening resistance to pathogens (Busby et al., 2016), and improving tolerance to abiotic stresses (Gill et al., 2016). Under saline conditions, DSE-mediated tolerance is classically attributed to modulation of phytohormone signaling, activation of antioxidant enzymes, and stimulation of osmolyte accumulation (Li et al., 2018; Pan et al., 2018; Yuan et al., 2016). However, most studies focus on mild to moderate salinity, where transient defense responses are sufficient. As salinity approaches the host tolerance threshold, these early-stage responses impose a substantial energetic toll, frequently leading to metabolic exhaustion and functional collapse of the symbiosis (Farias et al., 2020). Thus, enduring extreme ionic stress requires metabolic endurance: the capacity to sustain core energetic flux, structural renewal, and homeostatic balance over prolonged periods of extreme stress.

Suaeda salsa, an annual obligate halophyte (Flowers and Colmer, 2008), serves as a stringent model to examine this concept. This species exhibits a pronounced capacity to sequester Na^+ into vacuoles and constitutively accumulates compatible solutes for osmotic adjustment and ROS detoxification (Anjum et al., 2014; Bello et al., 2021; Ding et al., 2023). Because *S. salsa* possesses such a robust basal defense, DSE-mediated enhancement under extreme salinity cannot rely on upregulating basic stress responses; the symbiont must instead fundamentally recalibrate the hosts underlying metabolic endurance.

DSE isolates from distinct habitats deploy divergent metabolic strategies (Fracetto et al., 2023; Santos et al., 2021). Our previous work showed that DSE strains from semi-arid grasslands improved plant tolerance to high temperature, drought, and moderate salinity (Bi and Xue, 2023; Bi et al., 2024; Ren et al., 2024). However, whether non-adapted DSEs can support host plants under extreme Na_2SO_4-dominated salinity remains unknown. High-throughput metabolomics provides a systems-level framework to map these endurance networks(van Zelm et al., 2020; Yang et al., 2024). While previous studies have highlighted osmoregulatory and antioxidant compounds(Gupta et al., 2020; Sharma et al., 2019), isolated metabolic snapshots do not capture systemic resilience. An integrative approach combining metabolomics with ionomic profiling, root structural analysis, and rhizosphere functional assessment is essential to understand how distinct symbioses fail or endure under extreme environmental pressure.

To address this critical knowledge gap, we employed *S. salsa* to systematically contrast the functional trajectories of two DSE strains with differing ecological origins—a locally adapted strain (*Alternaria chlamydospora* SC11) and a non-adapted strain (*Alternaria* sp. As17463)—across a severe Na_2SO_4 gradient (0–0.4 M). Na_2SO_4 was selected as the stress source because the habitat from which SC11 was isolated is characterized predominantly by sulfate-based salinity (Zhang et al., 2021). We quantified plant growth, ion partitioning, root structural integrity, shoot metabolomic reprogramming, and rhizosphere nutrient and enzyme dynamics. We hypothesized that while both strains may activate early defensive responses, only a habitat-adapted strain can sustain metabolic endurance by maintaining coordinated ion homeostasis, nutrient cycling, and nucleotide- and sugar-mediated biosynthetic networks under extreme salinity. By integrating multi-level physiological and metabolic analyses, this work seeks to establish metabolic endurance as a defining determinant of symbiotic resilience in highly saline environments.

Materials and Methods

Experimental strains

A DSE strain isolated from the roots of Stipa krylovii collected from grassland adjacent to the Shengli open-pit mine in Xilinhot, Inner Mongolia, China, was deposited in the China General Microbiological Culture Collection Center under accession number CGMCC No. 17463 and is designated As17463 in the present study. A salt-tolerant DSE strain, *Alternaria chlamydospora*, isolated from the root system of *S. salsa* growing in the Hongshaquan mining area of Qitai County, Xinjiang, China, was deposited in the China General Microbiological Culture Collection Center under accession number CGMCC No. 42796 and is designated SC11 in the present study.

Medium and culture conditions

Potato dextrose agar and potato dextrose (PD) broth were used as the basal media for fungal cultivation. DSE strains were initially grown on PDA plates at 28°C for 12 days. Subsequently, agar plugs (approximately 5 mm in diameter) excised from the actively growing margins were transferred into 250-mL culture bottles containing 100 mL of PD broth and incubated at 28°C for an additional 12 days under static conditions.

Experimental design

To investigate the regulatory effects of salt-tolerant (SC11) and salt-sensitive (As17463) DSE strains on the salt tolerance of *S. salsa*, a controlled pot experiment was conducted. Seeds of *S. salsa* were surface-sterilized by immersion in 10% (v/v) H_2O_2 for 10 min, repeated three times, followed by thorough rinsing with sterile distilled water. Plastic pots (approximately 1.2 L capacity) were filled with 1.5 kg of sterilized river sand (particle size < 2 mm).

Thirty seeds were sown per pot, and seedlings were subsequently thinned to maintain ten uniform plants per pot. The sterilized sand contained 2.89 mg g^{-1} organic matter, 0.63 mg g^{-1} total nitrogen (TN), and 0.12 mg g^{-1} Na^{+}, with an initial pH of 8.2. Fresh DSE mycelia were harvested after 8 days of liquid culture, rinsed with sterile water, and gently blotted dry using sterile filter paper to remove excess surface moisture. For fungal inoculation, 10 g (fresh weight) of DSE mycelia were thoroughly mixed into each designated pot, whereas control treatments (CK) received an equivalent amount of autoclaved mycelial biomass.

The experiment followed a two-factor completely randomized block design, consisting of three inoculation treatments (CK, As17463, and SC11) and four salinity levels (0, 0.1, 0.2, and 0.4 M Na_2SO_4), with four biological replicates per treatment, yielding a total of 48 pots. All pots were maintained in a greenhouse under controlled conditions with a day/night temperature regime of 27°C/22°C and a 14-h/10-h light/dark photoperiod. Soil moisture was maintained at approximately 65% of maximum water-holding capacity by regular irrigation using the weighing method. Salt stress treatments were imposed throughout the entire growth period.

This experimental framework was designed to enable a comprehensive assessment of antioxidant physiological responses, leaf metabolic profiles of *S. salsa* under salinity stress, and key enzyme activities in the rhizosphere soil, thereby elucidating the potential mechanisms by which DSE colonization modulated host plant salt tolerance.

Analysis of plant samples

Plant phenotypic indicators

Plant height was measured using a tape measure. After 4 months of growth, *S. salsa* plants from each pot were harvested and separated into aboveground and belowground components. Root and shoot fresh biomasses were determined using an electronic balance, and total plant biomass was calculated as the sum of these components.

DSE colonization rate analysis

Fresh roots of *S. salsa* were gently washed with deionized water and cut into 0.5-cm segments. Root samples were cleared in 10% (w/v) potassium hydroxide (KOH) solution and subsequently stained with 0.5% (w/v) acid magenta following the method of Phillips and Hayman (1970). Fungal colonization was quantified using the slide method described by Biermann and Linderman (2006). For each sample, 30 randomly selected root segments were examined under light microscopy at 20× and 40× magnification. Total colonization rate, hyphal colonization rate, and microsclerotia colonization rate were calculated separately and expressed as the percentage of colonized root segments relative to the total number of segments observed.

Scanning electron microscopy (SEM) observation of root structure

Root segments (approximately 1 cm) were fixed in FAA solution, dehydrated through a graded ethanol series, and critical-point dried using tert-butanol. Dried specimens were sputter-coated with gold prior to SEM observation.

Plant nutrient content analysis

Shoots and roots were harvested separately and ground into fine powder. For total phosphorus (P) determination, samples were digested using concentrated sulfuric acid (H_2SO_4) in combination with H_2O_2, diluted, and filtered through a 0.22-μm membrane prior to analysis by inductively coupled plasma (ICP) spectrometry (Wang et al., 2021). Total carbon and TN contents were measured using an elemental analyzer (Vario MACRO cube, Elementar, Germany) following established procedures (Fang et al., 2021).

Potassium (K^+) and sodium (Na^+) concentrations in root and shoot tissues were quantified using inductively coupled plasma optical emission spectrometry (ICP-OES; Optima 2100 DV, PerkinElmer, USA). Plant samples were oven-dried at 60°C for 72 h and subsequently ground to a fine powder using a ball mill. Approximately 0.1 g of dried material was digested with 5 mL of 65% (v/v) nitric acid at 90°C for 6–8 h. The resulting digests were diluted with distilled water and analyzed by ICP-OES as described previously (Shen et al., 2024). Each treatment included four biological replicates.

Osmotic and oxidative homeostasis

Soluble sugars were determined using the phenol–sulfuric acid method (Bi et al., 2024). Soluble protein was determined using the Bradford method (Bi and Xue, 2023).

Crude enzyme extracts were prepared by homogenizing approximately 0.1 g of fresh root or shoot tissue in 2 mL of phosphate buffer (pH 7.8). Crude enzyme extracts were prepared by homogenizing 0.1 g of fresh tissue in 50 mM sodium phosphate buffer (pH 7.8), followed by centrifugation at 10,000 × g for 15 min at 4°C. The supernatant was used immediately for enzyme activity assays. SOD, CAT, and peroxidase (POD) activities were determined following established protocols. POD activity was assayed based on guaiacol oxidation in the presence of H_2O_2, and enzyme activity was calculated from the formation rate of the colored product (Gupta et al., 2020). SOD activity was measured using the nitroblue tetrazolium (NBT) photochemical reduction method (Wang et al., 2025a), while CAT activity was quantified based on the rate of H_2O_2 decomposition (Wang et al., 2025a). Enzyme activities were expressed as units per gram fresh weight per minute (U g^{-1} FW min^{-1}). MDA content was quantified according to Bi et al. (2024), and expressed as mmol g^{-1} FW.

Metabolomics analysis of the shoot

Fresh shoot samples (0.3 g) from each treatment were accurately weighed, immediately frozen in liquid nitrogen, and homogenized to a fine powder. Metabolites were extracted by adding 80% (v/v) methanol, followed by ultrasonication for 20 min and centrifugation at 12,000 × g for 15 min. The resulting supernatants were filtered through 0.22-μm membranes prior to LC–MS analysis.

Untargeted metabolomic profiling was performed using an ACQUITY UltraPerformance Liquid Chromatography (UPLC) system coupled with a Xevo G2-XS quadrupole time-of-flight mass spectrometer (Waters, Milford, MA, USA). Chromatographic separation was achieved on an ACQUITY UPLC HSS T3 column (2.1 × 100 mm, 1.8 μm; Waters). The mobile phase consisted of 0.1% (v/v) formic acid in water (solvent A) and 0.1% (v/v) formic acid in acetonitrile (solvent B), with a flow rate of 0.3 mL min^{-1}. The gradient elution program was as follows: 0–1 min, 0% B; 1–9 min, 0–50% B; 9–12 min, 50–100% B; 12–13.5 min, 100% B; 13.5–14 min, 100–0% B; and 14–17 min, 0% B. The column temperature was maintained at 40°C, and the injection volume was 1 μL.

Mass spectrometric detection was conducted using an electrospray ionization (ESI) source operated in both positive and negative ion modes (ESI^+ and ESI^-), with a mass scan range of m/z 50–1,200. The ion source temperature was set to 120°C, the desolvation temperature to 400°C, the desolvation gas flow rate to 800 L h^{-1}, and the cone voltage to 40 V. Data acquisition was performed using MassLynx software (version 4.1; Waters). A pooled quality control (QC) sample, prepared by combining equal aliquots of all samples, was injected at regular intervals (once every 10 runs) to assess instrument stability and analytical reproducibility.

Raw LC–MS data were processed using Progenesis QI software (version 2.1; Nonlinear Dynamics, Newcastle upon Tyne, UK) for baseline correction, noise reduction, peak detection, deconvolution, retention time alignment, and signal normalization. Metabolite annotation was performed based on accurate mass matching and MS/MS fragmentation pattern comparisons against the Human Metabolome Database (HMDB) and the Natural Products Atlas (NPAtlas). Where available, MS/MS spectra were used to enhance annotation confidence. All reported metabolites were therefore considered putatively identified, corresponding to the Metabolomics Standards Initiative (MSI) level 2. Differential metabolites were screened using combined multivariate and univariate criteria, including variable importance in projection (VIP) > 1.5, $P < 0.05$, and coefficient of variation (CV) < 30%.

Soil sampling and measurements

Soil microbial biomass and available nutrient analysis

Soil microbial biomass carbon (MBC), microbial biomass nitrogen (MBN), and microbial biomass phosphorus (MBP) were quantified using the chloroform fumigation–extraction method as described by Vance et al. (1987) Fresh soil samples were subdivided into fumigated and non-fumigated subsamples. Following fumigation, MBC and MBN were extracted with 0.5 mol L^{-1} K_2SO_4, whereas MBP was extracted using 0.5 mol L^{-1} $NaHCO_3$. The resulting extracts were filtered and analyzed for dissolved

organic carbon (DOC), dissolved organic nitrogen (DON), and Olsen phosphorus (Olsen-P). DOC concentrations were determined using an elemental analyzer, while Olsen-P was measured by ICP spectrometry. MBC, MBN, and MBP were calculated as the differences between fumigated and corresponding non-fumigated samples (Cui et al., 2018). Soil organic carbon (SOC) content was determined using the potassium dichromate oxidation method following Chen et al. (2018).

Soil extracellular enzyme activity

Activities of soil extracellular enzymes were determined using a fluorometric microplate assay with enzyme-specific fluorescent substrates. The enzymes analyzed included β-1,4-glucosidase (BG), cellobiohydrolase (CBH), β-xylosidase (BX), N-acetyl-β-D-glucosaminidase (NAG), leucine aminopeptidase (LAP), and alkaline phosphatase (AP) (Bi et al., 2024). Soil samples were homogenized in buffer at a ratio of 1:125 (w v^{-1}), and 200 μL of the resulting suspension was dispensed into black 96-well microplates. Subsequently, 50 μL of the corresponding substrate solution was added to each well. Plates were incubated in darkness at 37°C for 4 h, after which enzymatic reactions were terminated by the addition of NaOH. Fluorescence was measured using a microplate reader with excitation at 360 nm and emission at 450 nm. Enzyme activities were expressed as nanomoles of substrate converted per gram of dry soil per hour (nmol g^{-1} h^{-1}).

Statistical analysis

Statistical analyses were conducted using SPSS Statistics 26.0 (IBM, Armonk, NY, USA) and R (version 4.5.0). Data normality and homogeneity of variance were assessed using the Shapiro–Wilk and Levene's tests, respectively. A two-way analysis of variance (ANOVA) was performed to evaluate the effects of salinity, inoculation, and their interaction. When significant effects were detected, means were compared using Tukey's honestly significant difference (HSD) test at $P < 0.05$. Metabolomic data processing and multivariate analyses were conducted using MetaboAnalyst 6.0. Differential metabolites were identified using the criteria of variable importance in projection (VIP) > 1.5, $P < 0.05$, and coefficient of variation (CV) < 30%. KEGG pathway enrichment analysis was performed using over-representation analysis based on a hypergeometric test, and P values were adjusted using the Benjamini–Hochberg false discovery rate (FDR) procedure. Redundancy analysis (RDA) and variation partitioning analysis (VPA) were performed using the vegan package in R, and the significance of RDA models was assessed using 999 permutations. Spearman correlation analysis was conducted to examine relationships between metabolites and environmental variables, with P values adjusted using the Benjamini–Hochberg FDR method. Partial correlation analysis controlling for salinity was performed using the ppcor package. Heatmaps and UpSet plots were generated using TBtools (v2.325), and bar charts were produced using Origin 2024. In graphical representations, different uppercase letters indicate significant differences among inoculation treatments within the same salinity level, whereas different lowercase letters indicate significant differences among salinity levels within the same inoculation treatment.

Results and Analysis

DSE strain SC11 confers enhanced salt tolerance and promotes plant growth under saline conditions

Previous studies on DSE fungi have demonstrated that certain strains can substantially improve plant performance under abiotic stress. For example, Bi et al. (2024) have reported that DSE inoculation significantly increases plant biomass accumulation and survival under drought conditions. Building on these findings, the present study comparatively assessed the effects of two DSE strains, SC11 and As17463, on plant salt tolerance by subjecting inoculated plants to progressively increasing salinity levels (0, 0.1, 0.2, and 0.4 M Na_2SO_4).

Under non-saline conditions (0 M Na_2SO_4), plants across all treatments, including the uninoculated control (CK), exhibited normal morphology with no discernible differences in growth or appearance (Fig. 1A). As salinity intensified, CK plants displayed pronounced stress symptoms, such as leaf chlorosis, wilting, and severe growth inhibition. In contrast, plants inoculated with SC11 retained greener foliage and greater structural integrity. At the highest salinity level (0.4 M Na_2SO_4), nearly all CK plants failed to survive. In contrast, a substantial proportion of SC11-inoculated plants remained viable, highlighting the markedly stronger salt tolerance conferred by SC11 compared with both As17463 and the control. Consistent with these observations, plant height declined sharply with increasing salinity across all treatments (Fig. 1B); however, the magnitude of reduction was significantly attenuated in SC11-inoculated plants. At 0.1 M and 0.2 M Na_2SO_4, SC11-treated plants exhibited significantly greater heights than those inoculated with As17463 or left uninoculated ($P < 0.05$). Even under severe salt stress (0.4 M Na_2SO_4), SC11-inoculated plants maintained superior height and overall vigor, underscoring their enhanced stress resilience.

Survival rates exhibited a similar trend (Fig. 1C). Under low salinity (0.1 M Na_2SO_4), survival remained high across all treatments. With increasing salt concentrations, survival declined rapidly in CK plants, whereas SC11-inoculated plants maintained significantly higher survival rates, reaching approximately 60–70% at 0.4 M Na_2SO_4. In contrast, the As17463 strain provided only moderate protection under comparable conditions. Differences in fungal colonization further elucidated strain-specific performance (Fig. 1D). Although overall colonization efficiency decreased slightly with increasing salinity, SC11 consistently achieved significantly higher root colonization rates than As17463 across all salt treatments ($P < 0.05$), indicating superior adaptability and colonization capacity under saline stress.

Patterns of biomass accumulation further substantiated the growth-promoting effect of SC11 (Figs. 1E–G). Both root dry weight (Fig. 1E) and shoot dry weight (Fig. 1F) declined under saline conditions; however, these reductions were significantly less pronounced in SC11-inoculated plants. Notably, at 0.2 M Na_2SO_4, shoot dry weight in the SC11 treatment was nearly twice that of the control. Consequently, total dry biomass (Fig. 1G) remained consistently highest in SC11-inoculated plants across the salinity gradient, particularly under severe stress (0.4 M Na_2SO_4), where CK plants exhibited negligible growth.

Collectively, the superior colonization efficiency and pronounced stress-mitigation effects observed in SC11-inoculated plants, relative to As17463, suggested that SC11 played a pivotal role in enhancing host salt tolerance, potentially through improved regulation of ion homeostasis and osmotic adjustment under saline conditions.

(A) Representative phenotypes of *S. salsa* plants inoculated with CK, SC11, or As17463 under 0–0.4 M Na_2SO_4. (B) Plant height. (C) Survival rate. (D) Intraradical infection rate of DSE fungi. (E–G) Dry biomass of roots, shoots, and the total plant, respectively. Different uppercase letters indicate statistically significant differences among inoculation treatments at the same salt concentration, whereas different lowercase letters indicate significant differences across salt concentrations within the same inoculation treatment. treatment.

Inoculation of SC11 enhances nutrient absorption and maintains C/N homeostasis under salt stress

Salinity strongly impacted shoot elemental composition, reflecting coordinated alterations in carbon assimilation, nitrogen status, nutrient stoichiometry, and mineral allocation (Fig. S1A–E). Under non-saline conditions (0 M Na_2SO_4), shoot C, N, P, and S concentrations were comparable across control (CK), As17463-, and SC11-inoculated plants (Fig. S1A–E). With increasing salinity, CK plants exhibited pronounced declines in nutrient accumulation, indicating impaired nutrient acquisition under salt stress. By contrast, fungal inoculation mitigated these reductions, with SC11-inoculated plants consistently maintaining higher elemental concentrations across the salinity gradient. Specifically, shoot carbon content in CK plants dropped sharply under saline conditions, whereas SC11-treated plants preserved significantly higher C levels at 0.2 and 0.4 M Na_2SO_4 ($P < 0.05$; Fig. S1A), reflecting improved carbon assimilation under stress. Shoot nitrogen content declined with rising salinity, yet SC11 inoculation sustained markedly higher N levels than CK and As17463 treatments, particularly at moderate stress (0.2 M Na_2SO_4; Fig. S1B). Consequently, the C/N ratio, which increased substantially in CK plants under salinity, remained relatively stable in SC11-treated plants (Fig. S1C), indicating maintenance of carbon–nitrogen stoichiometric balance. Salinity-induced reductions in shoot phosphorus and sulfur were also attenuated by fungal inoculation, with SC11-treated plants showing the highest P and S concentrations at elevated salinity (0.2–0.4 M Na_2SO_4; Fig. S1D–E). These findings collectively demonstrated that SC11 effectively preserved shoot elemental composition and nutrient homeostasis under salt stress, outperforming As17463 in maintaining plant nutritional status.

SC11 stabilizes Na^+/K^+ homeostasis under salinity

Given that ionic toxicity and Na^+/K^+ imbalance are central constraints on plant performance under salinity, we quantified shoot and root Na^+ and K^+ concentrations, as well as Na^+/K^+ ratios, to assess how SC11 modulated ion accumulation and balance across salinity levels (Fig. 2A–I). Shoot Na^+

concentrations increased with rising salinity in all treatments (Fig. 2A). At ≤ 0.1 M Na_2SO_4, SC11-inoculated plants exhibited a more moderate Na^+ increase than As17463-treated plants, likely reflecting biomass-driven dilution of intracellular Na^+. At ≥ 0.2 M salinity, however, SC11-treated plants accumulated significantly more Na^+ in shoots than both As17463 and CK plants, indicating a shift toward Na^+ sequestration rather than exclusion. Concurrently, shoot K^+ concentrations remained higher in SC11-inoculated plants at ≤ 0.2 M Na_2SO_4 (Fig. 2B), resulting in a lower Na^+/K^+ ratio compared with other treatments (Fig. 2C). At 0.4 M Na_2SO_4, both shoot Na^+ and the Na^+/K^+ ratio increased sharply across all treatments, though SC11 plants maintained appreciable K^+ levels.

Root Na^+ and K^+ concentrations mirrored shoot patterns (Fig. 2D–F), with root Na^+ surging markedly at 0.4 M. Given the role of roots in ion uptake and translocation to shoots, total Na^+ and K^+ accumulation were calculated to evaluate the impact of microbial inoculation. SC11-inoculated plants sequestered significantly more Na^+ in both roots and shoots across the salinity gradient than As17463-treated and uninoculated plants (0–0.4 M Na_2SO_4; Fig. 2G–H). Notably, at extreme salinity (0.4 M Na_2SO_4), SC11-treated plants accumulated approximately 2.1-fold more total Na^+ than CK while maintaining substantial biomass ($P < 0.05$). These results suggested that SC11 enhanced salt tolerance by prioritizing internal Na^+ reallocation and sequestration over external exclusion, aligning with halophyte adaptive strategies for tolerating high ionic loads. As a whole, SC11 represented a promising microbial candidate for phytoremediation in saline soils, offering a sustainable biological approach to rehabilitate salt-affected fields while supporting plant establishment under extreme salinity.

Inoculation of SC11 preserves root structure and promotes epidermal adaptation to stress in high-salinity environments

Root surface integrity and epidermal architecture are closely linked to plant performance under salinity stress; therefore, SEM was employed to examine root surface morphology and fungal colonization patterns in *S. salsa* inoculated with As17463 or SC11 across a Na_2SO_4 gradient (0–0.4 M) (Fig. S2). Under non-saline conditions (0 M), the root surfaces of all treatments (CK, As17463, and SC11) exhibited a smooth and intact texture, with distinct epidermal cell outlines and no visible external appendages. Upon exposure to moderate salt stress (0.1 M and 0.2 M Na_2SO_4), all groups underwent pronounced morphological alterations: the root epidermis became extensively decorated with flattened, hollow, ribbon-like structures. These formations appeared in both inoculated and uninoculated roots, indicating that they were plant-derived epidermal extensions, likely representing collapsed root hairs in response to stress, rather than fungal hyphae.

Fungal inoculation substantially influenced the persistence and structural integrity of roots under extreme salt stress. CK roots completely disintegrated at 0.4 M Na_2SO_4, resulting in total loss of

structural organization. In contrast, roots colonized by DSE fungi survived the high-salinity conditions. Notably, SC11-inoculated roots maintained robust structural integrity and exhibited a pronounced layer of hollow epidermal adaptations even at 0.4 M. Roots treated with As17463, however, displayed partial wilting and reduced epidermal coverage. These observations indicated that the formation of hollow epidermal structures represented an intrinsic adaptive response of the host plant to salinity, whereas colonization by SC11, and to a lesser extent As17463, was essential for preventing root senescence and preserving structural integrity in environments characterized by extreme salinity.

SC11 enhances antioxidant enzyme activity and facilitates the management of salt-induced stress

Oxidative damage and osmotic imbalance constitute central physiological constraints under salinity stress; therefore, lipid peroxidation, antioxidant enzyme activities, and compatible solute accumulation were quantified to assess treatment-dependent stress responses across an increasing Na_2SO_4 gradient (Fig. 3). Under non-saline conditions (0 M Na_2SO_4), plants across all treatments exhibited comparable levels of MDA, along with similar activities of SOD, CAT, and POD (Fig. 3A–D). As salinity intensified, however, distinct treatment-specific physiological divergences emerged. MDA, an established biomarker of membrane lipid peroxidation, rose sharply in the control plants, whereas both As17463- and SC11-inoculated plants maintained substantially lower MDA levels throughout the salinity gradient. Notably, SC11-inoculated plants consistently displayed the lowest MDA accumulation (Fig. 3A), reflecting superior mitigation of oxidative injury.

Under mild to moderate salinity (0.1–0.2 M Na_2SO_4), the activities of antioxidant enzymes (SOD, CAT, and POD) increased across all treatments; however, these activities declined precipitously in control plants at 0.4 M Na_2SO_4 (Fig. 3B–D). In contrast, both fungal inoculations sustained significantly higher antioxidant enzyme activities at all salinity levels, with SC11 eliciting the most pronounced enhancement, particularly at 0.2 M Na_2SO_4. These results indicated that SC11 more effectively activated the antioxidant defense cascade, thereby restraining Na_2SO_4-induced accumulation of ROS and enhancing cellular resilience.

Patterns of osmolyte accumulation mirrored these trends (Fig. 3E–F). Soluble protein and soluble sugar contents increased modestly in all treatments under 0.1–0.2 M Na_2SO_4 but declined substantially in the control at 0.4 M. Fungal inoculation significantly promoted the accumulation of compatible solutes under salt stress, with SC11-inoculated plants exhibiting the highest levels, most evident at 0.2 M Na_2SO_4. This enhanced solute buildup likely facilitated osmotic adjustment and conferred improved cellular protection under ionic stress conditions.

Taken together, these findings demonstrated that SC11 conferred heightened tolerance to Na_2SO_4-induced salinity by mitigating oxidative damage, sustaining robust antioxidant enzyme activities, and promoting compatible osmolyte accumulation. Through these integrated physiological adjustments,

SC11 supported cellular homeostasis, metabolic functionality, and overall stress resilience under saline conditions.

Inoculation of SC11 enhances nutrient availability and microbial abundance in salt-stressed soils

SOC, DOC, DON, and Olsen-P are key indicators reflecting soil nutrient cycling efficiency and the microbial-driven capacity for water and material exchange under saline–alkali stress (Hou et al., 2021; Li et al., 2024; Liao et al., 2024). As core components of the soil carbon pool, the stability of SOC and DOC directly influences soil water-holding capacity and ionic buffering potential. DON and Olsen-P serve as immediate nitrogen and phosphorus sources for plants, and their dynamic fluctuations are closely tied to the balance between microbial mineralization and sequestration processes(Huang et al., 2025). Salt stress typically inhibits organic matter decomposition and nutrient release through osmotic effects and ionic toxicity, leading to deterioration of soil physicochemical properties (Rietz and Haynes, 2003). In contrast, salt-tolerant microorganisms, such as certain DSE fungi, can alleviate such stress by secreting extracellular polymers, promoting soil aggregate formation, and enhancing enzymatic activity, thereby sustaining carbon and nitrogen cycling stability (Zhang et al., 2024a). The present study aimed to evaluate the capacity of DSE strains SC11 and As17463 to modulate nitrogen cycling and microbial activity in saline soils by monitoring changes in soil physicochemical and microbial parameters following inoculation.

To determine the influence of fungal inoculation on nitrogen cycling and rhizosphere microbial activity, we measured a suite of soil physicochemical and microbiological properties under a gradient of Na_2SO_4 concentrations (Fig. S3). Under non-saline conditions (0 M Na_2SO_4), all treatments displayed similar levels of SOC, DOC, and DON (Fig. S3A–C). With increasing salinity, SOC and DOC in CK soils declined significantly, indicating that salt stress slowed the decomposition and turnover of soil organic matter. By contrast, soils associated with SC11-inoculated plants maintained substantially higher SOC and DOC levels across all salinity treatments, reflecting more efficient carbon incorporation and stabilization under saline stress. Although As17463 inoculation provided some improvement, its effects were consistently inferior to those of SC11. Similarly, Olsen-P levels in CK soils decreased sharply with rising salinity, whereas SC11 inoculation prevented this decline, maintaining elevated Olsen-P even at 0.4 M Na_2SO_4 (Fig. S3D).

As expected, soil electrical conductivity (EC) increased with salinity in all treatments. Notably, under moderate salinity, SC11-inoculated soils exhibited lower EC values compared with CK soils, indicating superior ionic regulation in the rhizosphere (Fig. S3E). Soil pH remained relatively stable across treatments (Fig. S3F). Microbial biomass indicators followed analogous trends (Fig. S3G–I). In CK soils, increasing salinity caused rapid reductions in MBC, MBN, and MBP, reflecting inhibited microbial metabolism under salt-induced stress. In contrast, SC11 inoculation significantly mitigated these losses, maintaining the highest MBC, MBN, and MBP across all salinity levels. These results indicated that SC11

not only enhanced rhizosphere nutrient retention but also sustained microbial biomass and extracellular enzyme activity, thereby improving functional capacity under saline conditions.

SC11 inoculation enhanced organic-matter retention and microbial activity under salt stress, stabilizing nutrient pools and supporting a rhizosphere environment favorable for plant salt tolerance.

Inoculation of SC11 enhances rhizosphere enzymatic activity and supports nutrient cycling under salt stress

To elucidate the functional processes in the rhizosphere that underpin fungal-mediated salt tolerance, the activities of six key soil enzymes involved in carbon, nitrogen, and phosphorus cycling were quantified (Fig. 4). LAP and NAG mediate nitrogen cycling, AP contributes to phosphorus mobilization, and BG, CBH, and BX participate in carbon degradation. Under non-saline conditions (0 M Na_2SO_4), soils inoculated with SC11 displayed LAP, NAG, and AP activities comparable to, or slightly exceeding, those of CK and As17463 treatments, indicating that fungal colonization modestly enhanced basal enzymatic function (Fig. 4A–C).

With increasing salinity, enzyme activities in CK soils declined sharply, reflecting substantial inhibition of microbial metabolism and nutrient cycling under salt stress. In contrast, SC11 inoculation markedly maintained or elevated LAP and NAG activities across the salinity gradient (Fig. 4A–B), suggesting enhanced microbial proficiency in organic nitrogen decomposition and nitrogen mineralization. Similarly, AP activity (Fig. 4C) remained consistently elevated in SC11-inoculated soils, implying that phosphorus mobilization from organic sources was effectively sustained under saline conditions. Activities of carbon-degrading enzymes, BG, CBH, and BX, were strongly suppressed in CK and As17463 treatments under higher salinity (Fig. 4D–F). Conversely, SC11 treatments consistently maintained high or stable enzyme activity, particularly for BG and BX, highlighting the strain's ability to preserve carbon metabolism in the rhizosphere even under severe salt stress. This effect likely reflected the promotion of a more dynamic and metabolically capable microbial community proficient in degrading complex polysaccharides. Overall, these results indicated that SC11 inoculation preserved or enhanced enzymatic activity under salt stress, thereby maintaining carbon, nitrogen, and phosphorus cycling and contributing to improved nutrient availability. The functional stability of the rhizosphere microbiome mediated by SC11 likely enhanced plant nutrient acquisition and salt tolerance.

Metabolomic profiling of *S. salsa* under salt stress (0–0.4 M Na_2SO_4) was conducted to uncover the divergent strategies and underlying mechanisms employed by DSE strains SC11 and As17463. PCA showed clear separation of metabolic profiles between inoculation treatments across the salinity gradient (Fig. S4). At 0 M Na_2SO_4, PC1 and PC2 explained 41.3% and 22.9% of the variance, respectively (Fig. S4A). At 0.2 M, the variance accounted for by PC1 and PC2 increased to 64.3% and 22.5% (Fig. S4B), while at 0.4 M, they represented 61% and 20% of the total variation (Fig. S4C). These patterns indicated strain-specific metabolic adjustments under increasing salt stress.

Detailed metabolite analysis revealed that in the absence of salt, As17463 inoculation upregulated 1,097 metabolites and downregulated 631, whereas SC11 upregulated 638 and downregulated 355 (Fig. S5A–B). At 0.2 M Na_2SO_4, As17463 modulated 1,113 metabolites upward and 1,130 downward, while SC11 altered 972 upward and 593 downward (Fig. S5C–D). At the highest salinity (0.4 M), As17463 influenced 517 upregulated and 386 downregulated metabolites, whereas SC11 induced 955 upregulated and 1,040 downregulated metabolites (Fig. S5E–F). UpSet analysis further clarified strain-specific metabolic signatures: under no salt, As17463 uniquely regulated 713 upregulated and 366 downregulated metabolites, while SC11 specifically modulated 239 upregulated and 106 downregulated compounds (Fig. S4D). At 0.2 M, As17463 uniquely altered 620 upregulated and 400 downregulated metabolites, versus 271 and 71 for SC11, respectively (Fig. S4E). At 0.4 M, SC11 exhibited a dramatic increase in unique metabolic regulation with 642 upregulated and 764 downregulated metabolites, compared to 189 and 125 for As17463 (Fig. S4F). Hierarchical clustering revealed two distinct metabolic trajectories: As17463-infected plants initially exhibited metabolic upregulation followed by decline as salinity intensified, whereas SC11-inoculated plants displayed progressively enhanced metabolic responses with increasing salinity levels (Fig. S6).

Together, the sustained rhizosphere enzymatic activity and the extensive, salinity-responsive metabolic reprogramming in the host plant demonstrate that SC11 supports *S. salsa* salt tolerance through integrated rhizosphere and systemic mechanisms, outperforming As17463.

Metabolomic differentiation between As17463 and SC11 inoculation under graded salt stress in S. salsa

Comprehensive metabolomic profiling revealed that inoculation with either DSE strain, As17463 or SC11, profoundly reconfigured the metabolic landscape of *S. salsa* across three Na_2SO_4 concentrations (0, 0.2, and 0.4 M) (Fig. 5). Despite distinct regulatory intensities, both symbionts shared several conserved metabolic patterns, including elevated accumulation of lipids and lipid-like molecules (LLP), organic acids and derivatives (OAD), benzenoids, and phenylpropanoids and polyketides (PP), coupled with reduced levels of organoheterocyclic compounds (OC) and organic oxygen compounds (OOC). These shared shifts suggested that both DSEs enhanced osmotic adjustment, lipid remodeling, and antioxidant metabolism, core mechanisms underpinning DSE-mediated salt tolerance. Notably, the presence of these changes even under non-saline conditions indicated a form of “metabolic priming”, preconditioning host tissues for imminent stress.

Although both strains broadly influenced similar metabolite categories, their regulatory dynamics diverged markedly along the salinity gradient. Under non-saline conditions, As17463-inoculated plants exhibited consistently higher abundances of LLP, OAD, OC, PP, benzenoids, and OOC relative to SC11-inoculated plants (Fig. 5A right; Fig. 5B right). Conversely, SC11 induced a more pronounced upregulation of LLP compared to As17463, 40.6% versus 33.2%, respectively (Fig. 5A left; Fig. 5B left). At 0.2 M Na_2SO_4, As17463 elicited a substantial increase in downregulated LLP-related differentially accumulated metabolites (DAMs), exceeding the number of upregulated ones. Simultaneously, OAD, OC, PP,

benzenoids, and OOC accumulated to higher absolute levels in the As17463 treatment than in SC11 (Fig. 5C right; Fig. 5D right). Interestingly, however, the proportional upregulation of OAD, OC, benzenoids, and OOC was significantly higher in SC11-inoculated plants than in those treated with As17463 (Fig. 5C left; Fig. 5D left).

At the highest salinity (0.4 M Na_2SO_4), the magnitude of upregulated DAM abundance in LLP, OAD, OC, PP, benzenoids, and OOC was comparable between the two DSE strains (Fig. 5E left; Fig. 5F left); however, the total number of DAMs was markedly greater in SC11 than in As17463 (Fig. 5E right; Fig. 5F right). Notably, SC11 induced substantially more upregulated alkaloid-related DAMs than As17463, with 19 and six DAMs, respectively, highlighting a broader metabolic responsiveness under extreme stress.

Metabolic pathway analysis further revealed functional distinctions: As17463 primarily activated lipid and phenylpropanoid metabolism, reflecting a defense-oriented metabolic state, whereas SC11 enhanced organic nitrogen and nucleoside metabolism, indicative of nutrient reallocation and homeostatic optimization. At moderate salinity (0.2 M Na_2SO_4), As17463 triggered widespread metabolic activation, particularly in lipids, benzenoids, and organic acids, consistent with rapid osmolyte synthesis and ROS detoxification. By contrast, SC11 elicited a more selective yet balanced response, characterized by targeted upregulation of nitrogen and phosphorus pathways, reflecting an energy-efficient regulatory mode.

A striking divergence emerged under severe salinity (0.4 M Na_2SO_4): the number of DAMs in As17463-inoculated plants declined sharply, whereas SC11-inoculated plants exhibited a dramatic increase in both the number and diversity of DAMs. This pattern indicated that SC11 became metabolically dominant under high stress, activating an expanded suite of protective pathways, including organic acids, phenylpropanoids, and lipid derivatives. These results suggested that As17463 primarily functioned as an early-stage “metabolic activator”, initiating defense metabolism, whereas SC11 operated as a “metabolic stabilizer”, sustaining long-term redox balance, nutrient homeostasis, and cellular protection when osmotic and ionic stresses intensify.

Panels A–F show functional category distribution and abundance ratios of DAMs in pairwise comparisons between CK and the fungal inoculations: As17463 (A, C, E) and SC11 (B, D, F) under 0 M (A, B), 0.2 M (C, D), and 0.4 M (E, F) Na_2SO_4. Left panels indicate the proportion (%) of upregulated (orange) and downregulated (blue) metabolites within each chemical class. Right panels display the total number of DAMs per category.

Differential pathway enrichment patterns in S. salsa inoculated with DSE strains As17463 and SC11 under varying salt stress

To dissect the functional mechanisms by which DSE strains As17463 and SC11 regulate host responses to salt stress, KEGG pathway enrichment analysis was conducted on DAMs for each treatment group. The results revealed that *S. salsa* inoculated with these DSEs underwent substantial metabolic reprogramming across the Na_2SO_4 gradient (Fig. S7). Both As17463 and SC11 significantly modulated a

wide array of primary and secondary metabolic pathways, yet their regulatory dynamics differed markedly depending on the intensity of salt stress.

Under non-saline conditions (0 M Na_2SO_4), fungal inoculation induced distinctive metabolic shifts indicative of “priming”. As17463 triggered broad upregulation across multiple metabolic activities, significantly enriching pathways related to nucleotide and lipid homeostasis, including purine metabolism, pyrimidine metabolism, porphyrin metabolism, and biosynthesis of unsaturated fatty acids. In contrast, SC11 elicited a more targeted response, selectively enriching porphyrin metabolism and caffeine metabolism. Both strains exhibited significant downregulation of retinol metabolism relative to CK, suggesting a shared remodeling of secondary metabolic processes upon fungal colonization.

At moderate salinity (0.2 M Na_2SO_4), the metabolic trajectories of the two strains diverged substantially, particularly within nucleotide metabolism. In As17463-inoculated plants, caffeine metabolism, purine metabolism, and vitamin B6 metabolism were upregulated, whereas pyrimidine metabolism was notably suppressed. By contrast, SC11-inoculated plants displayed distinct upregulation of pyrimidine metabolism and phosphonate and phosphinate metabolism, suggesting a strategic prioritization of nucleotide sugar precursors critical for cell wall maintenance. This highlighted a fundamental difference between the strains: SC11 promoted structural reinforcement under stress, while As17463 downregulated pathways necessary for such maintenance.

The most pronounced distinctions emerged under severe salinity (0.4 M Na_2SO_4). As17463-inoculated plants exhibited a fragmented metabolic response, with upregulation largely confined to retinol metabolism, one-carbon pool by folate, and purine metabolism, accompanied by downregulation of ether lipid metabolism. This pattern indicated a limited capacity to sustain broad metabolic functions under extreme stress. In stark contrast, SC11-inoculated plants maintained coordinated and robust upregulation of pathways essential for structural integrity and energetic homeostasis. Key enriched pathways included glycerophospholipid metabolism and biosynthesis of unsaturated fatty acids, indicative of active membrane remodeling to counter lipid peroxidation. Porphyrin metabolism remained elevated, supporting the synthesis of cofactors for antioxidant enzymes, while purine metabolism was also sustained. Concurrent upregulation of steroid hormone biosynthesis further emphasized SC11’s role in modulating growth and stress signaling.

Overall, KEGG enrichment suggests that SC11 elicits a more coordinated metabolic response under severe salinity. In contrast to the comparatively fragmented pathway activation observed for As17463 at 0.4 M Na_2SO_4, SC11 sustained membrane- and energy-related processes—including glycerophospholipid metabolism and unsaturated fatty-acid biosynthesis—while maintaining porphyrin and purine metabolism to support cofactor availability and redox homeostasis, together with upregulation of steroid hormone biosynthesis. This homeostatic stabilization likely contributes to the enhanced salt tolerance of SC11-inoculated plants.

Differential pathway analysis of As17463 and SC11 inoculation under salt stress in S. salsa

KEGG pathway analysis revealed pronounced differences in the regulation of metabolic networks between As17463 and SC11 inoculation in *S. salsa*, particularly in response to increasing salinity (Fig. 6). Both DSE strains induced substantial shifts across a spectrum of metabolic pathways; however, the patterns and intensity of activation were clearly strain- and salt concentration–dependent.

Under non-saline conditions (0 M Na_2SO_4), both As17463 and SC11 enhanced key metabolic pathways, including glycerophospholipid metabolism, amino acid biosynthesis, and glycolysis/gluconeogenesis (Fig. 6). These pathways are critical for maintaining cellular membrane integrity, energy production, and nitrogen assimilation, highlighting a shared role of DSEs in optimizing basal metabolism to support nutrient uptake and stress preparedness. Both strains also upregulated phenylpropanoid biosynthesis pathways, indicative of increased production of secondary metabolites implicated in antioxidative defense. This common metabolic activation suggested that both As17463 and SC11 enhanced the plant's capacity to mitigate oxidative stress and maintain cellular homeostasis even under non-saline conditions.

At moderate salinity (0.2 M Na_2SO_4), the metabolic responses diverged distinctly, reflecting strain-specific strategies in coping with osmotic stress. As17463 inoculation strongly activated lipid metabolism, particularly sphingolipid biosynthesis, and amino acid metabolism, with notable enrichment of UDP-sugar–associated carbohydrate metabolism. These metabolic shifts were consistent with observed increases in antioxidant enzyme activities and osmolyte accumulation in As17463-colonized plants, reflecting a coordinated reprogramming that stabilized membranes and facilitated ROS detoxification. In contrast, SC11 inoculation selectively enhanced nitrogen metabolism and phosphonate/phosphinate metabolism, indicating a targeted strategy prioritizing nitrogen assimilation and the maintenance of metabolic balance under moderate salt stress. Furthermore, SC11-treated plants showed upregulation of glycogen biosynthesis and pyruvate metabolism, suggesting optimized energy utilization and enhanced metabolic stability.

Under severe salinity (0.4 M Na_2SO_4), the metabolic trajectories of the two strains exhibited a striking reversal. As17463-treated plants displayed a marked reduction in the number of significantly enriched pathways, particularly within lipid and amino acid metabolism, signaling a collapse of broad metabolic activation. This implied that As17463 might shift its functional focus toward alternative processes, such as ion homeostasis or stress avoidance, under extreme salt stress rather than sustaining generalized metabolic reprogramming. In stark contrast, SC11-inoculated plants demonstrated a dramatic increase in both the number and diversity of enriched pathways, including lipid remodeling (notably sphingolipid metabolism), glycolysis/gluconeogenesis, and key antioxidant pathways such as glutathione metabolism. The sustained and expansive activation of these pathways under high salinity indicated that

SC11 functioned as a dominant stabilizer of metabolic homeostasis, supporting energy efficiency, oxidative protection, and long-term cellular resilience during prolonged osmotic and ionic stress.

Together, these findings indicate that As17463 and SC11 deploy complementary, salinity-dependent metabolic programs in *S. salsa*: As17463 preferentially up-regulates defense-related lipid and antioxidant pathways under moderate salinity (0.2 M Na_2SO_4), whereas SC11 maintains a broader network supporting energy metabolism, membrane lipid remodeling, and glutathione-mediated redox balance under severe salinity (0.4 M). This partitioning of functions across the salinity gradient likely underpins the wide salt tolerance of *S. salsa*.

Schematic of DSE strain–mediated enhancement of salt tolerance in S. salsa under salt stress

To elucidate the molecular mechanisms by which the two DSE strains modulated host salt tolerance, we constructed an integrated metabolic network based on differential pathway enrichment analyses (Fig. 7). Under salt stress, both As17463 and SC11 remodeled lipid metabolism, upregulated glycan biosynthesis, and activated cofactor, vitamin, and purine metabolic processes. Additionally, both strains elevated the levels of key metabolites, including ADP-Glc, UDP-GlcNAc, GDP-L-Fucose, and coproporphyrinogen III, the latter of which was positively correlated with POD and CAT activities.

Pronounced strain-specific regulatory patterns were also evident. As17463 selectively promoted terpenoid and polyketide metabolism (including brassinosteroid biosynthesis) while suppressing the biosynthesis of specific secondary metabolites and sterol skeleton components. In contrast, SC11 strongly induced pyrimidine metabolism (characterized by uridine accumulation) while downregulating cutin, suberin, wax biosynthesis, and arachidonic/α-linolenic acid metabolism.

Interplay among metabolites, physiological traits, and soil variables under salt stress

To unravel the complex interplay between DAMs and plant antioxidant capacity, soil salinity, nutrients, and extracellular enzymes, we initially conducted a Spearman correlation analysis (Fig. 8A). The results revealed that Uroporphyrinogen I and GDP-L-fucose exhibited robust positive correlations with antioxidant enzymes (CAT, SOD) and soluble proteins, whereas Ganglioside GA2 (d18:1/12:0) and 9,10-Epoxy-18-hydroxystearate displayed contrasting negative associations with these functional parameters. Furthermore, stress indicators such as soluble sugars and MDA were significantly and positively correlated with metabolites involved in pyrimidine and purine metabolism, with the notable exception of UMP. Conversely, soil-related parameters—specifically β-glucosidase (BG), alkaline phosphatase (AP), and DOC—exhibited significant negative associations with metabolites linked to pyrimidine and nucleotide metabolism.

While the correlation analysis unveiled specific pairwise interactions, to elucidate the system-wide multivariate response patterns of different inoculation treatments (CK, SC11, As17463) across the salinity gradient (0, 0.2, 0.4 M), a RDA was performed (Fig. 8B). The first two canonical axes explained 66.83% of the total variance (RDA1: 40.89%; RDA2: 25.94%). The biplot demonstrated that spatial segregation of samples was cooperatively driven by salinity stress (dominating the first axis) and inoculation status (dominating the second axis). Notably, the strong positive loading of conductivity along RDA1 unequivocally indicates that the salinity gradient acts as the primary environmental driver pulling samples to the right along the primary axis. Under the baseline non-saline condition (0 M), all treatments (uninoculated CK, SC11, and As17463) showed no distinct differentiation, clustering tightly in the top-left quadrant. This baseline state was positively correlated with specific hydrolase activities (AP.Ab, BG.Ab, CBH.Ab) and DOC, and was enriched in metabolites such as guanine and UMP. With the introduction of salt stress, the metabolic and physiological trajectories of the treatments underwent significant niche differentiation. The CK and SC11 treatments under moderate stress (0.2 M), alongside the As17463 treatment under severe stress (0.4 M), exhibited a convergent response, shifting towards the bottom-left quadrant—a trajectory primarily driven by P.Ab, coproporphyrinogen III, and 22-hydroxydocosanoic acid. In stark contrast, specific inoculations that successfully mitigated salt stress displayed entirely distinct spatial topological features. Under 0.2 M stress, the As17463 treatment formed an independent cluster in the top-right quadrant, robustly driven by the activation of antioxidant defense systems (POD, CAT) and the accumulation of specific metabolites (GDP-L-fucose, SAICAR, and CDP-ethanolamine). Under 0.4 M stress, the SC11 treatment segregated along the positive RDA1 axis (near RDA2 = 0), aligning closely with the accumulation of uric acid. Furthermore, although no samples clustered in the bottom-right quadrant, this region was heavily populated by typical stress-damage markers (MDA, sugar, and hypoxanthine) whose loadings positioned diametrically opposite to the non-stressed control group. Collectively, these results demonstrate that specific fungal inoculations (As17463 and SC11) can decouple the linear stress effects imposed by the salinity gradient, fundamentally altering the host's physiological response trajectory by specifically reconfiguring its antioxidant and metabolic networks.

Building upon these complex multivariate networks, to quantitatively disentangle the relative contributions of external soil environments and internal host physiology to the overall metabolomic variation, we utilized VPA (Fig. 8C). These variables collectively accounted for an impressive 88.37% of the total metabolic variance. Strikingly, soil-related variables acted as the dominant independent driver, explaining 39.45% of the variation, whereas plant physiological variables independently accounted for only 5.21%. Crucially, the analysis unveiled a massive shared fraction (43.71%) between the two sets of variables. This substantial overlap mechanistically corroborates the spatial associations observed in the RDA, quantitatively demonstrating that under salinity and inoculation treatments, the alteration of soil microecology and the physiological response of the host plant do not occur in isolation; rather, they are governed by an intensely synergistic coupling mechanism.

Discussion

Persistent colonization as the ecological foundation of SC11-mediated salt tolerance

DSEs are increasingly recognized as important regulators of plant performance under a wide range of environmental stresses, including salinity, drought, and nutrient limitation (Bi et al., 2024; Tan et al., 2024). Numerous studies have demonstrated that DSE inoculation can improve plant growth, nutrient acquisition, and osmotic adjustment under low-to-moderate salinity(Bi et al., 2024; Farias et al., 2020). Nevertheless, the extent to which these beneficial effects are maintained under severe salinity remains highly strain dependent and is still poorly understood (Huertas et al., 2024). Using *S. salsa* as a model, two DSE isolates displayed divergent salinity-response trajectories, with SC11 maintaining functional benefits under severe salinity (0.4 M Na_2SO_4) whereas As17463 declined. This sustained tolerance was associated with coordinated plant–soil functional network regulation across multiple physiological and metabolic dimensions.

Among all measured variables, persistent root colonization appeared to provide the ecological foundation for the superior performance of SC11. Colonization by SC11 remained relatively stable even under severe salinity, whereas colonization by As17463 declined progressively with increasing salt concentration. Stable colonization likely facilitates continuous resource exchange, signaling interactions, and metabolic feedbacks between host and symbiont (Gill et al., 2016). Stable colonization was accompanied by greater stoichiometric stability in the host(Gill et al., 2016). In the absence of stable physical contact, any beneficial metabolic or physiological effect that an endophyte might otherwise confer is likely to diminish as stress intensifies(Barrow, 2003; Gonçalves et al., 2021; Zuo et al., 2020). The consequences of this difference in colonization stability were reflected in host elemental homeostasis(Gonzalez Mateu et al., 2020; Gupta et al., 2020). SC11-inoculated plants maintained more consistent shoot C, N, P, and S concentrations, together with less variation in C/N ratios across the salinity gradient. This stoichiometric stability indicates that carbon assimilation and nutrient metabolism remained more tightly coordinated in SC11-inoculated plants than in uninoculated controls, in which salinity frequently disrupts elemental balance (Tufail et al., 2021). Similar relationships between DSE colonization stability and host nutrient regulation have been reported in other plant–fungal symbioses exposed to environmental stress (Farias et al., 2020), further supporting the interpretation that colonization persistence is a prerequisite for sustained functional benefits.

Differences in ion regulation between the two strains provided additional evidence that SC11 maintained a qualitatively different physiological state under severe salinity. Under moderate salinity, SC11-inoculated plants maintained higher K^+ concentrations and lower Na^+/K^+ ratios than uninoculated controls, consistent with a Na^+ exclusion strategy. Under severe salinity, however, SC11-inoculated plants accumulated substantial Na^+ while maintaining growth and physiological activity. This pattern suggests a transition from active Na^+ exclusion toward tissue-level accommodation and intracellular compartmentalization. Recent evidence indicates that when salinity exceeds approximately 100 mM NaCl, vacuolar Na^+ sequestration becomes more important than SOS1-mediated efflux as a mechanism

for mitigating ionic toxicity, reflecting a systemic reconfiguration of ion transport priorities under extreme stress (Cheema et al., 2025). Endophytic symbionts have been shown to modulate ion transport systems associated with this transition, including upregulation of NHX1 expression to enhance vacuolar Na^+ compartmentalization efficiency (Gupta et al., 2020; Liang et al., 2024). (Molina-Montenegro et al., 2018). Critically, SC11-inoculated plants maintained stable K^+, N, and P concentrations despite substantial Na^+ accumulation, indicating that essential nutrient acquisition was effectively decoupled from Na^+-induced ionic toxicity. This decoupling suggests a system-level reprogramming of ion homeostasis in which Na^+ sequestration does not compromise the nutrient balance required for sustained growth and metabolism (Salt et al., 2008; Saradadevi et al., 2021) (Wang et al., 2020). Taken together, the coordinated maintenance of colonization stability, elemental stoichiometry, and ion homeostasis under severe salinity indicates that SC11 established a functional symbiotic state that As17463 was unable to sustain, and that this stability provided the ecological foundation for the superior host performance observed at high salinity.

SC11 and As17463 represent distinct strategies of salinity adaptation

The contrasting physiological and metabolomic profiles of SC11- and As17463-inoculated plants suggest that these two strains employ fundamentally different strategies for coping with salinity stress. Characterizing these strategies precisely is important because it reveals that effective DSE-mediated tolerance need not follow a single conserved pathway. Under moderate salinity, As17463 induced broad activation of pathways associated with oxidative defense and stress signaling, including amino acid metabolism and vitamin B_6 metabolism. Vitamin B_6 vitamers function not only as metabolic cofactors but also as potent antioxidants that protect against oxidative damage (Chen et al., 2024). Together with elevated antioxidant enzyme activities, these responses indicate that As17463 primarily promotes salt tolerance through rapid activation of classical defense mechanisms—a strategy well-suited to acute or moderate stress but potentially limited in its capacity to sustain performance under prolonged severe conditions. SC11, by contrast, elicited a comparatively selective response under moderate salinity but maintained a substantially broader metabolic capacity under severe salinity. Pathways related to pyrimidine metabolism, nitrogen metabolism, phosphate metabolism, glutathione metabolism, membrane lipid biosynthesis, and central carbon metabolism remained active even at 0.4 M Na_2SO_4. Because these pathways collectively support nucleotide synthesis, biosynthetic repair, energy metabolism, redox regulation, and membrane maintenance, their sustained activity is likely to contribute to the preservation of cellular homeostasis under prolonged stress (Hildebrandt, 2018; Obata and Fernie, 2012). Under severe salinity, the metabolic profile of As17463 contracted toward a smaller set of survival-related pathways, whereas SC11 retained broader metabolic functionality. Sustained membrane lipid remodeling supports membrane stability and cellular function under saline conditions, while glutathione metabolism contributes directly to ROS detoxification and redox buffering (Guo et al., 2019). These observations indicate that the two DSE strains represent alternative adaptive strategies. As17463

follows a rapid-response strategy characterized by strong early activation of defense-related pathways, whereas SC11 adopts a sustained-resilience strategy centered on long-term maintenance of metabolic homeostasis and biosynthetic capacity. The persistence of metabolic functionality, rather than the magnitude of the initial stress response, therefore appears to be a critical determinant of long-term symbiotic effectiveness under extreme salinity (Gonçalves et al., 2021; Li et al., 2017).

Pyrimidine metabolism may function as a central hub linking metabolism, structural maintenance, and stress tolerance

Among the metabolic features that distinguished SC11 from As17463, the consistent enrichment of pyrimidine metabolism was particularly notable. Unlike many pathways that responded transiently to salinity, pyrimidine metabolism remained enriched across all stress levels in SC11-inoculated plants and was accompanied by increased accumulation of uridine and other pyrimidine-related metabolites. This sustained enrichment warrants careful interpretation because it points toward a metabolic function that extends well beyond nucleic acid synthesis. Pyrimidine metabolism is traditionally regarded primarily as a source of nucleotides for DNA and RNA synthesis(Zheng et al., 2024). However, emerging evidence indicates that pyrimidine-derived metabolites contribute to stress adaptation through at least two additional mechanisms. First, enhanced nucleotide turnover may facilitate cellular repair and maintenance under stress conditions by sustaining the supply of biosynthetic precursors required for damaged macromolecule replacement (Ebert and Orellana, 2025; Rinne et al., 2024). Second, pyrimidine metabolism generates UDP-sugars that serve as essential substrates for polysaccharide biosynthesis and glycosylation reactions, thereby directly supporting cell-wall construction and remodeling under stress (Ebert and Orellana, 2025; Guo et al., 2024a; Wang et al., 2025a). This pathway is particularly significant in the present context because it connects several otherwise independent lines of evidence. The sustained enrichment of pyrimidine metabolism is consistent with the maintenance of nucleotide homeostasis, the preservation of cell-wall integrity observed anatomically in SC11-inoculated roots, and the accumulation of nucleotide-sugar metabolites discussed in the following section. Previous transcriptomic and metabolomic studies have reported positive associations between enhanced pyrimidine metabolism and salinity tolerance (Chen et al., 2025; Li et al., 2024). supporting the interpretation that this pathway plays an active rather than merely reactive role in stress adaptation. Although direct metabolic flux measurements were not performed in the present study, the repeated and consistent enrichment of pyrimidine metabolism under severe salinity strongly suggests that maintenance of nucleotide metabolism represents a central and functionally integrative component of the SC11-mediated tolerance strategy.

Nucleotide-sugar metabolism links metabolic reprogramming to root structural integrity

Closely related to the enrichment of pyrimidine metabolism was the consistent accumulation of nucleotide-sugar metabolites in DSE-inoculated plants. UDP-GlcNAc, ADP-glucose, and GDP-L-fucose accumulated following inoculation with both fungal strains, irrespective of fungal identity, indicating that enhanced nucleotide-sugar metabolism represents a general feature of the DSE–*S. salsa* association rather than a strain-specific response. However, the functional consequences of this metabolic shift differed between strains, particularly under severe salinity. Each of these metabolites contributes to a distinct but interconnected aspect of stress adaptation. UDP-GlcNAc serves as an essential substrate for protein and lipid glycosylation, processes that contribute to membrane stability and the maintenance of protein function under saline conditions (Chen and Cheng, 2024; Ebert and Orellana, 2025). ADP-glucose provides precursors for carbon storage and compatible solute synthesis, thereby supporting osmotic adjustment (Kirsch et al., 2019; Ortega-Martinez et al., 2023). GDP-L-fucose participates in rhamnogalacturonan II biosynthesis and cell-wall cross-linking, processes associated with mechanical stability and water retention during osmotic stress (O'Neill et al., 2001; Waszczak et al., 2024). Collectively, these metabolites indicate enhanced capacity for cell-wall biosynthesis, glycosylation, carbon allocation, and osmotic adjustment—processes that are all relevant to survival under severe ionic stress. The functional significance of this metabolic activity is supported by root anatomical observations. Under moderate salinity, epidermal collapse was observed across all treatments, suggesting a general osmotic adaptation. Under severe salinity, however, root structural integrity diverged substantially among treatments. Uninoculated plants exhibited extensive tissue deterioration, whereas SC11-inoculated roots largely retained their structural organization. This preservation likely reflects the combined effects of improved ionic regulation and continued synthesis of structural metabolites required for cell-wall maintenance and repair (Dangi et al., 2018; Liu et al., 2022). Although cell-wall composition was not directly quantified, the metabolomic data indicate that nucleotide-sugar metabolism remained active in SC11-treated plants under severe salinity, potentially supporting continuous cell-wall repair and reinforcement (Cosgrove, 2024; Guo et al., 2024b). These findings collectively demonstrate that metabolic reprogramming contributes to salt tolerance not only through osmotic and antioxidant regulation but also through the active preservation of root structural integrity—a dimension of stress adaptation that has received comparatively little attention in studies of DSE symbioses.

Salt tolerance as a system-level property of the soil–root–plant continuum

Colonization stability, ionic regulation, metabolic resilience, and structural maintenance provide mechanistic explanations for the enhanced salt tolerance observed in SC11-treated plants. However, our multivariate analyses revealed that these responses were embedded within a broader, tightly coupled soil–root–plant system, and that understanding them in isolation may underestimate the true basis of DSE-mediated salt tolerance. Variance partitioning demonstrated that soil and plant variables explained substantial and largely overlapping fractions of metabolomic variability. The large shared component between soil and plant datasets is particularly informative because it indicates that host metabolism

and rhizosphere functioning are not independent under saline conditions(Berendsen et al., 2012). Rather, the two components appear to form an integrated adaptive system in which changes in one compartment are propagated throughout the entire plant–soil continuum(Bever et al., 2010). Similar cross-compartment feedbacks are increasingly recognized as critical determinants of plant performance under environmental stress (Bandopadhyay et al., 2024; Jin et al., 2024). A plausible mechanistic explanation for this coupling is as follows. Persistent fungal colonization modifies rhizosphere biochemical processes, influencing nutrient availability, extracellular enzyme activities, and microbial resource turnover(van der Heijden et al., 2015). Enhanced nutrient acquisition subsequently supports greater metabolic activity within the host, enabling maintenance of biosynthetic pathways associated with cellular repair and stress adaptation(Munns and Gilliham, 2015). In turn, metabolically active plants sustain larger carbon fluxes to the rhizosphere, reinforcing microbial activity and extracellular enzyme production(Sasse et al., 2018). Such bidirectional feedbacks are consistent with the sustained β-glucosidase and alkaline phosphatase activities observed in SC11-associated soils, and with emerging evidence that root-derived carbon inputs play a central role in regulating microbial functioning under saline conditions (Zhang et al., 2024b). Within this framework, the superior performance of SC11 under severe salinity reflects not simply a superior host physiological response, but rather an ability to maintain functional connectivity across biological compartments even when salinity reaches levels that destabilize the As17463 symbiosis. Salt tolerance, in this view, is best understood as a system-level emergent property of coordinated interactions among fungal persistence, host metabolic reprogramming, and rhizosphere processes—rather than as the outcome of any single physiological mechanism acting in isolation.

Several limitations should nevertheless be acknowledged. The present study primarily identifies associations among colonization, metabolism, physiology, and soil processes, and therefore does not establish direct causal relationships. In particular, ion compartmentalization, metabolite fluxes, and molecular signaling pathways were not directly quantified. Future studies integrating isotope tracing, transcriptomics, proteomics, and targeted functional assays will be valuable for determining how specific metabolic pathways contribute to stress tolerance and how these pathways are coordinated between host plants and their microbial partners.

Conclusions and conceptual implications

The results of this study demonstrate that the superior performance of SC11 under severe salinity cannot be attributed to any single physiological mechanism. Instead, it reflects the coordinated maintenance of multiple interacting processes, including colonization stability, ionic and nutrient homeostasis, pyrimidine and nucleotide-sugar metabolism, root structural integrity, and rhizosphere functionality, across an increasing salinity gradient. We therefore propose that DSE-mediated salt tolerance is most accurately understood as a system-level phenomenon, in which fungal persistence enables and sustains coordinated interactions among host metabolic reprogramming, ionic regulation, and soil biochemical processes. Under conditions that progressively destabilized the As17463 symbiosis, SC11 promoted host resilience by maintaining metabolic and functional connectivity across

the soil–root–plant continuum. Collectively, these findings provide a mechanistic basis for selecting habitat-adapted DSE inoculants and highlight the importance of maintaining integrated plant-soil-microbe functions for the restoration and sustainable management of saline environments.

Declarations

Declaration of Competing Interest

The authors declare that they have no known competing financial interests or personal relationships that could have influenced the work reported in this paper.

Acknowledgments

We sincerely thank the editor and reviewers for their insightful comments and constructive feedback on earlier versions of this manuscript. This work was supported by the Major Science and Technology Special Project of Xinjiang Uygur Autonomous Region (2025A01004-2) and the National Natural Science Foundation of China (52394194).

Data Availability

The data that support the findings of this study are available from the corresponding author upon reasonable request.

References

1. Abhayawickrama B, Gimhani D, Kottearachchi N, Herath V, Liyanage D, Senadheera P (2020) In Silico Identification of QTL-Based Polymorphic Genes as Salt-Responsive Potential Candidates through Mapping with Two Reference Genomes in Rice. Plants (Basel) 9
2. Anjum NA, Ahmad I, Válega M, Mohmood I, Gill SS, Tuteja N, Duarte AC, Pereira E (2014) Salt Marsh Halophyte Services to Metal–Metalloid Remediation: Assessment of the Processes and Underlying Mechanisms. Crit Rev Environ Sci Technol 44:2038–2106
3. Bandopadhyay S, Li X, Bowsher AW, Last RL, Shade A (2024) Disentangling plant- and environment-mediated drivers of active rhizosphere bacterial community dynamics during short-term drought. Nat Commun 15:6347
4. Barrow JR (2003) Atypical morphology of dark septate fungal root endophytes of Bouteloua in arid southwestern USA rangelands. Mycorrhiza 13:239–247
5. Bello SK, Alayafi AH, Al-Solaimani SG, Abo-Elyousr KAM (2021) Mitigating Soil Salinity Stress with Gypsum and Bio-Organic Amendments: A Review. Agronomy 11

6. Berendsen RL, Pieterse CM, Bakker PA (2012) The rhizosphere microbiome and plant health. Trends Plant Sci 17:478–486
7. Bever JD, Dickie IA, Facelli E, Facelli JM, Klironomos J, Moora M, Rillig MC, Stock WD, Tibbett M, Zobel M (2010) Rooting theories of plant community ecology in microbial interactions. Trends Ecol Evol 25:468–478
8. Bi Y, Xue Z (2023) Dark septate endophyte inoculation enhances antioxidant activity in Astragalus membranaceus var. mongholicus under heat stress. Physiol Plant 175:e14054
9. Bi YL, Tan H, Zhang SS, Kang JP (2024) Response Mechanism of Extracellular Polymeric Substances Synthesized by Alternaria sp. on Drought Stress in Alfalfa (Medicago sativa L). J Agric Food Chem 72:16812–16824
10. Biermann B, Linderman RG (2006) Quantifying Vesicular-Arbuscular Mycorrhizae: A Proposed Method Towards Standardization *. New Phytol 87:63–67
11. Cheema RA, Rehman HM, Nawaz S, Ahmad S, Lam HM (2025) Deciphering the Sodium Sensing Mechanisms in Glycophytes and Halophytes. Plant Cell Environ 48:8586–8603
12. Chen L, Liu L, Mao C, Qin S, Wang J, Liu F, Blagodatsky S, Yang G, Zhang Q, Zhang D, Yu J, Yang Y (2018) Nitrogen availability regulates topsoil carbon dynamics after permafrost thaw by altering microbial metabolic efficiency. Nat Commun 9:3951
13. Chen Y, Dan Z, Li S (2024) GROWTH REGULATING FACTOR 7-mediated arbutin metabolism enhances rice salt tolerance. Plant Cell 36:2834–2850
14. Chen YH, Cheng WH (2024) Hexosamine biosynthesis and related pathways, protein N-glycosylation and O-GlcNAcylation: their interconnection and role in plants. Front Plant Sci 15:1349064
15. Chen Z, Wang P, Zhao S, Sun Y, Liu Y, Chen S, Chen W, Zhao G, Wei G, Chen C (2025) Functionalized Silica Nanoparticles Mitigate Salt Stress in Soybean: Comprehensive Insights of Physiological, Metabolomic, and Microbiome Responses. J Agric Food Chem 73:10814–10825
16. Cosgrove DJ (2024) Structure and growth of plant cell walls. Nat Rev Mol Cell Biol 25:340–358
17. Cui Y, Fang L, Guo X, Wang X, Zhang Y, Li P, Zhang X (2018) Ecoenzymatic stoichiometry and microbial nutrient limitation in rhizosphere soil in the arid area of the northern Loess Plateau, China. Soil Biol Biochem 116:11–21
18. Dangi AK, Sharma B, Khangwal I, Shukla P (2018) Combinatorial Interactions of Biotic and Abiotic Stresses in Plants and Their Molecular Mechanisms: Systems Biology Approach. Mol Biotechnol 60:636–650
19. De Castro O, Innangi M, Menale B, Carfagna S (2018) O-acetylserine(thio)lyase (OAS-TL) molecular expression in Pancratium maritimum L. (Amaryllidaceae) under salt stress. Planta 247:773–777
20. Ding Z, Liu Z, Bao J, Wang Y, Li J, Wang Q, Tian X (2023) Transcriptomic study of Suaeda salsa in response to salt and drought stress. Funct Plant Biol 50:765–776
21. Ebert B, Orellana A (2025) Nucleotide Sugar Transporters: Orchestrating Luminal Glycosylation in Plants. Annu Rev Plant Biol 76:53–83

22. Fang Z, Han X, Xie M, Jiao F (2021) Spatial Distribution Patterns and Driving Factors of Plant Biomass and Leaf N, P Stoichiometry on the Loess Plateau of China. Plants (Basel) 10
23. Farias GC, Nunes KG, Soares MA, de Siqueira KA, Lima WC, Neves ALR, de Lacerda CF, Filho EG (2020) Dark septate endophytic fungi mitigate the effects of salt stress on cowpea plants. Braz J Microbiol 51:243–253
24. Flowers TJ, Colmer TD (2008) Salinity tolerance in halophytes. New Phytol 179:945–963
25. Fracetto GGM, Fracetto FJC, de Souza ER, de Araújo VLVP, Lidelias M, Mendes Júnior JP, da Silva CCG (2023) Microbial inoculants and their potential application in salinity management. In: Sharma VK, Kumar A, Passarini MRZ, Parmar S, Singh VK (eds) Microbial Inoculants. Academic, pp 53–74
26. Gill SS, Gill R, Trivedi DK, Anjum NA, Sharma KK, Ansari MW, Ansari AA, Johri AK, Prasad R, Pereira E, Varma A, Tuteja N (2016) Piriformospora indica: Potential and Significance in Plant Stress Tolerance. Front Microbiol 7:332
27. Gonçalves DR, Pena R, Zotz G, Albach DC (2021) Effects of fungal inoculation on the growth of Salicornia (Amaranthaceae) under different salinity conditions. Symbiosis 84:195–208
28. Gonzalez Mateu M, Baldwin AH, Maul JE, Yarwood SA (2020) Dark septate endophyte improves salt tolerance of native and invasive lineages of *Phragmites australis*. ISME J 14:1943–1954
29. Grünig CR, Queloz V, Sieber TN (2011) Structure of Diversity in Dark Septate Endophytes: From Species to Genes. In: Pirttilä AM, Frank AC (eds) Endophytes of Forest Trees. Springer Netherlands, Dordrecht, pp 3–30
30. Guo J, Zhou Y, Guo H, Min W (2024a) Cotton adapts to Na2SO4 stress by regulating the metabolic intensity and distribution of metabolites in roots and leaves. Ind Crops Prod 215
31. Guo Q, Liu L, Barkla BJ (2019) Membrane Lipid Remodeling in Response to Salinity. Int J Mol Sci 20
32. Guo W, Chen J, Liu L, Ren Y, Guo R, Ding Y, Li Y, Chai J, Sun Y, Guo C (2024b) MsMIOX2, encoding a MsbZIP53-activated myo-inositol oxygenase, enhances saline-alkali stress tolerance by regulating cell wall pectin and hemicellulose biosynthesis in alfalfa. Plant J 120:998–1013
33. Gupta S, Schillaci M, Walker R, Smith PMC, Watt M, Roessner U (2020) Alleviation of salinity stress in plants by endophytic plant-fungal symbiosis: Current knowledge, perspectives and future directions. Plant Soil 461:219–244
34. Hildebrandt TM (2018) Synthesis versus degradation: directions of amino acid metabolism during Arabidopsis abiotic stress response. Plant Mol Biol 98:121–135
35. Hou L, Li X, He X, Zuo Y, Zhang D, Zhao L (2021) Effect of dark septate endophytes on plant performance of Artemisia ordosica and associated soil microbial functional group abundance under salt stress. Appl Soil Ecol 165
36. Huang Y, Tang S, Liu R, Yu P, Liu J, Xiao T, Zhang Y, Fan M, Zhang F, Ni B (2025) Soil organic carbon mediates plant immunity-rhizosphere microbiome interactions and controls colonization resistance to microbial inoculants. Cell Host Microbe 33, 1929–1944 e1927

37. Huertas V, Jimenez A, Dianez F, Chelhaoui R, Santos M (2024) Importance of Dark Septate Endophytes in Agriculture in the Face of Climate Change. J Fungi (Basel) 10
38. Ivushkin K, Bartholomeus H, Bregt AK, Pulatov A, Kempen B, de Sousa L (2019) Global mapping of soil salinity change. Remote Sens Environ 231:111260–111283
39. Jin X, Jia H, Ran L, Wu F, Liu J, Schlaeppi K, Dini-Andreote F, Wei Z, Zhou X (2024) Fusaric acid mediates the assembly of disease-suppressive rhizosphere microbiota via induced shifts in plant root exudates. Nat Commun 15:5125
40. Kaya C, Ugurlar F, Ashraf M, Alyemeni MN, Dewil R, Ahmad P (2024) Mitigating salt toxicity and overcoming phosphate deficiency alone and in combination in pepper (Capsicum annuum L.) plants through supplementation of hydrogen sulfide. J Environ Manage 351:119759
41. Kirsch F, Klahn S, Hagemann M (2019) Salt-Regulated Accumulation of the Compatible Solutes Sucrose and Glucosylglycerol in Cyanobacteria and Its Biotechnological Potential. Front Microbiol 10:2139
42. Knapp DG, Kovacs GM, Zajta E, Groenewald JZ, Crous PW (2015) Dark septate endophytic pleosporalean genera from semiarid areas. Persoonia 35:87–100
43. Li M, Zhou W, Sun M, Shi W, Lun J, Zhou B, Hou L, Gao Z (2024) Decoupling soil community structure, functional composition, and nitrogen metabolic activity driven by salinity in coastal wetlands. Soil Biol Biochem 198
44. Li X, He X, Hou L, Ren Y, Wang S, Su F (2018) Dark septate endophytes isolated from a xerophyte plant promote the growth of Ammopiptanthus mongolicus under drought condition. Sci Rep 8:7896
45. Li X, Ma L, Bu N, Li Y, Zhang L (2017) Endophytic infection modifies organic acid and mineral element accumulation by rice under Na2CO3 stress. Plant Soil 420:93–103
46. Liang X, Li J, Yang Y, Jiang C, Guo Y (2024) Designing salt stress-resilient crops: Current progress and future challenges. J Integr Plant Biol 66:303–329
47. Liao L, Wang J, Dijkstra FA, Lei S, Zhang L, Wang X, Liu G, Zhang C (2024) Nitrogen enrichment stimulates rhizosphere multi-element cycling genes via mediating plant biomass and root exudates. Soil Biol Biochem 190
48. Liu J, Shao Y, Feng X, Otie V, Matsuura A, Irshad M, Zheng Y, An P (2022) Cell Wall Components and Extensibility Regulate Root Growth in Suaeda salsa and Spinacia oleracea under Salinity. Plants (Basel) 11
49. Molina-Montenegro MA, Acuña-Rodríguez IS, Torres-Díaz C, Gundel PE (2018) Root endophytes improve physiological performance and yield in crops under salt stress by up-regulating the foliar sodium concentration. bioRxiv
50. Munns R, Gilliham M (2015) Salinity tolerance of crops - what is the cost? New Phytol 208:668–673
51. Negacz K, Bruning B, Vellinga P (2021) Achieving multiple sustainable development goals through saline agriculture, Future of Sustainable Agriculture in Saline Environments. CRC, pp 13–28

52. O'Neill MA, Eberhard S, Albersheim P, Darvill AG (2001) Requirement of borate cross-linking of cell wall rhamnogalacturonan II for Arabidopsis growth. Science 294:846–849
53. Obata T, Fernie AR (2012) The use of metabolomics to dissect plant responses to abiotic stresses. Cell Mol Life Sci 69:3225–3243
54. Ortega-Martinez P, Roldan M, Diaz-Troya S, Florencio FJ (2023) Stress response requires an efficient connection between glycogen and central carbon metabolism by phosphoglucomutases in cyanobacteria. J Exp Bot 74:1532–1550
55. Pan X, Qin Y, Yuan Z (2018) Potential of a halophyte-associated endophytic fungus for sustaining Chinese white poplar growth under salinity. Symbiosis 76:109–116
56. Phillips JM, Hayman DS (1970) Improved procedures for clearing roots and staining parasitic and vesicular-arbuscular mycorrhizal fungi for rapid assessment of infection. Trans Br Mycological Soc 55:158–IN118
57. Ren Y, Bi Y, Kang J (2024) The overlooked salt: Impact of dark septate endophytes on alfalfa at varying sodium sulfate levels. Rhizosphere 32
58. Rietz DN, Haynes RJ (2003) Effects of irrigation-induced salinity and sodicity on soil microbial activity. Soil Biol Biochem 35:845–854
59. Rinne J, Niehaus M, Medina-Escobar N, Straube H, Schaarschmidt F, Rugen N, Braun HP, Herde M, Witte CP (2024) Three Arabidopsis UMP kinases have different roles in pyrimidine nucleotide biosynthesis and (deoxy)CMP salvage. Plant Cell 36:3611–3630
60. Rodriguez RJ, White JF Jr., Arnold AE, Redman RS (2009) Fungal endophytes: diversity and functional roles. New Phytol 182:314–330
61. Saddhe AA, Manuka R, Nikalje GC, Penna S (2020) Halophytes as a Potential Resource for Phytodesalination. In: Grigore M-N (ed) Handbook of Halophytes. Springer International Publishing, Cham, pp 1–21
62. Salt DE, Baxter I, Lahner B (2008) Ionomics and the study of the plant ionome. Annu Rev Plant Biol 59:709–733
63. Santos M, Cesanelli I, Diánez F, Sánchez-Montesinos B, Moreno-Gavíra A (2021) Advances in the Role of Dark Septate Endophytes in the Plant Resistance to Abiotic and Biotic Stresses. Journal of Fungi. MDPI AG, p 939
64. Saradadevi GP, Das D, Mangrauthia SK, Mohapatra S, Chikkaputtaiah C, Roorkiwal M, Solanki M, Sundaram RM, Chirravuri NN, Sakhare AS, Kota S, Varshney RK, Mohannath G (2021) Genetic, Epigenetic, Genomic and Microbial Approaches to Enhance Salt Tolerance of Plants: A Comprehensive Review. Biology 10
65. Sasse J, Martinoia E, Northen T (2018) Feed Your Friends: Do Plant Exudates Shape the Root Microbiome? Trends Plant Sci 23:25–41
66. Sharma A, Shahzad B, Rehman A, Bhardwaj R, Landi M, Zheng B (2019) Response of Phenylpropanoid Pathway and the Role of Polyphenols in Plants under Abiotic Stress. Molecules 24

67. Shen T, Xu F, Chen D, Yan R, Wang Q, Li K, Zhang G, Ni L, Jiang M (2024) A B-box transcription factor OsBBX17 regulates saline-alkaline tolerance through the MAPK cascade pathway in rice. New Phytol 241:2158–2175
68. Sun Y, Kong X, Li C, Liu Y, Ding Z (2015) Potassium Retention under Salt Stress Is Associated with Natural Variation in Salinity Tolerance among Arabidopsis Accessions. PLoS ONE 10:e0124032
69. Tan H, Bi Y, Zhang S, Kang J, Wang K, Wang D (2025) Soil–microbiome–plant interactions mediated by dark septate endophytes and extracellular polymeric substances drive ecological restoration in open-pit dumps. Rhizosphere 36
70. Tan JY, Yue ZC, Li ST, Pan YY, Chu ZY, Ban YH, Xu ZY (2024) Alleviation of Salt Stress and Changes in Glycyrrhizic Acid Accumulation by Dark Septate Endophytes in Glycyrrhiza glabra Grown under Salt Stress. J Agric Food Chem 72:14557–14569
71. Tufail MA, Bejarano A, Shakoor A, Naeem A, Arif MS, Dar AA, Farooq TH, Pertot I, Puopolo G (2021) Can Bacterial Endophytes Be Used as a Promising Bio-Inoculant for the Mitigation of Salinity Stress in Crop Plants?-A Global Meta-Analysis of the Last Decade (2011–2020). Microorganisms 9.
72. Usuki F, Narisawa K (2007) A mutualistic symbiosis between a dark septate endophytic fungus, *Heteroconium chaetospira*, and a nonmycorrhizal plant, Chinese cabbage. Mycologia 99:175–184
73. van der Heijden MGA, Martin FM, Selosse MA, Sanders IR (2015) Mycorrhizal ecology and evolution: the past, the present, and the future. New Phytol 205:1406–1423
74. van Zelm E, Zhang Y, Testerink C (2020) Salt Tolerance Mechanisms of Plants. Annu Rev Plant Biol 71:403–433
75. Vance ED, Brookes PC, Jenkinson DS (1987) An extraction method for measuring soil microbial biomass C. Soil Biol Biochem 19:703–707
76. Wang C, Wei X, Wang Y, Wu C, Jiao P, Jiang Z, Liu S, Ma Y, Guan S (2025a) Metabolomics and Transcriptomic Analysis Revealed the Response Mechanism of Maize to Saline-Alkali Stress. Plant Biotechnol J 23:5397–5416
77. Wang G, Yao K, Harindintwali JD, Jho EH, Hu J, Sun M (2025b) Assembly Patterns and Functional Roles of Bacterial Generalists and Specialists in the Remediation of Saline-Alkali Soils. Environ Microbiol Rep 17, e70221
78. Wang K, Bi Y, Cao Y, Peng S, Christie P, Ma S, Zhang J, Xie L (2021) Shifts in composition and function of soil fungal communities and edaphic properties during the reclamation chronosequence of an open-cast coal mining dump. Sci Total Environ 767:144465
79. Wang W-Y, Liu Y-Q, Duan H-R, Yin X-X, Cui Y-N, Chai W-W, Song X, Flowers TJ, Wang S-M (2020) SsHKT1;1 is coordinated with SsSOS1 and SsNHX1 to regulate Na+ homeostasis in Suaeda salsa under saline conditions. Plant Soil 449:117–131
80. Waszczak C, Yarmolinsky D, Leal Gavarron M, Vahisalu T, Sierla M, Zamora O, Carter R, Puukko T, Sipari N, Lamminmaki A, Durner J, Ernst D, Winkler JB, Paulin L, Auvinen P, Fleming AJ, Andersson MX, Kollist H, Kangasjarvi J (2024) Synthesis and import of GDP-l-fucose into the Golgi affect plant-water relations. New Phytol 241:747–763

81. Yang W, Wen D, Yang Y, Li H, Yang C, Yu J, Xiang H (2024) Metabolomics and transcriptomics combined with physiology reveal key metabolic pathway responses in tobacco roots exposed to NaHS. BMC Plant Biol 24:680
82. Yuan Z, Druzhinina IS, Labbe J, Redman R, Qin Y, Rodriguez R, Zhang C, Tuskan GA, Lin F (2016) Specialized Microbiome of a Halophyte and its Role in Helping Non-Host Plants to Withstand Salinity. Sci Rep 6:32467
83. Zhang G, Bai J, Zhai Y, Jia J, Zhao Q, Wang W, Hu X (2024a) Microbial diversity and functions in saline soils: A review from a biogeochemical perspective. J Adv Res 59:129–140
84. Zhang H, Hu M, Ma H, Jiang L, Zhao Z, Ma J, Wang L (2021) Differential Responses of Dimorphic Seeds and Seedlings to Abiotic Stresses in the Halophyte Suaeda salsa. Front Plant Sci 12:630338
85. Zhang S, Bi Y, Tan H (2025) Dark septate endophytic fungus Alternaria sp. 17463 regulates various antioxidant enzymes and compounds to mitigate salt stress caused by different anion salts. J Biotechnol 401:48–59
86. Zhang W, Yang S, Wei T, Su Y (2024b) Enhancing Photosynthetic Carbon Transport in Rice Plant Optimizes Rhizosphere Bacterial Community in Saline Soil. Int J Mol Sci 25
87. Zheng Y, Cao X, Zhou Y, Ma S, Wang Y, Li Z, Zhao D, Yang Y, Zhang H, Meng C, Xie Z, Sui X, Xu K, Li Y, Zhang CS (2024) Purines enrich root-associated Pseudomonas and improve wild soybean growth under salt stress. Nat Commun 15:3520
88. Zuo Y, Su F, He X, Li M (2020) Colonization by dark septate endophytes improves the growth of Hedysarum scoparium under multiple inoculum levels. Symbiosis 82:201–214

Figures

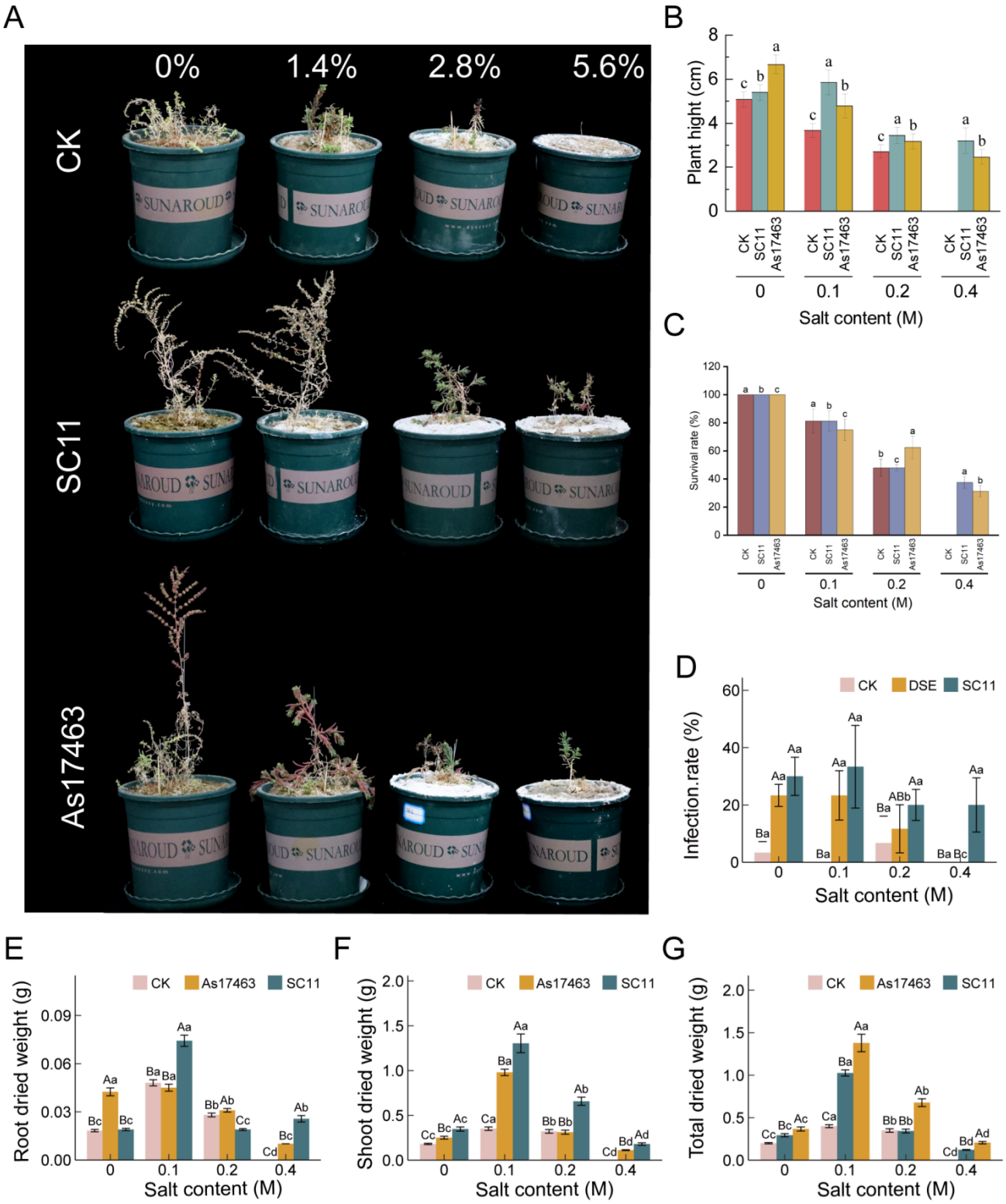

Figure 1

Effects of DSE fungi on plant growth and salt tolerance under varying Na_2SO_4 concentrations.

(A) Representative phenotypes of *S. salsa* plants inoculated with CK, SC11, or As17463 under 0–0.4 M Na_2SO_4. (B) Plant height. (C) Survival rate. (D) Intraradical infection rate of DSE fungi. (E–G) Dry biomass of roots, shoots, and the total plant, respectively. Different uppercase letters indicate statistically

significant differences among inoculation treatments at the same salt concentration, whereas different lowercase letters indicate significant differences across salt concentrations within the same inoculation treatment. treatment.

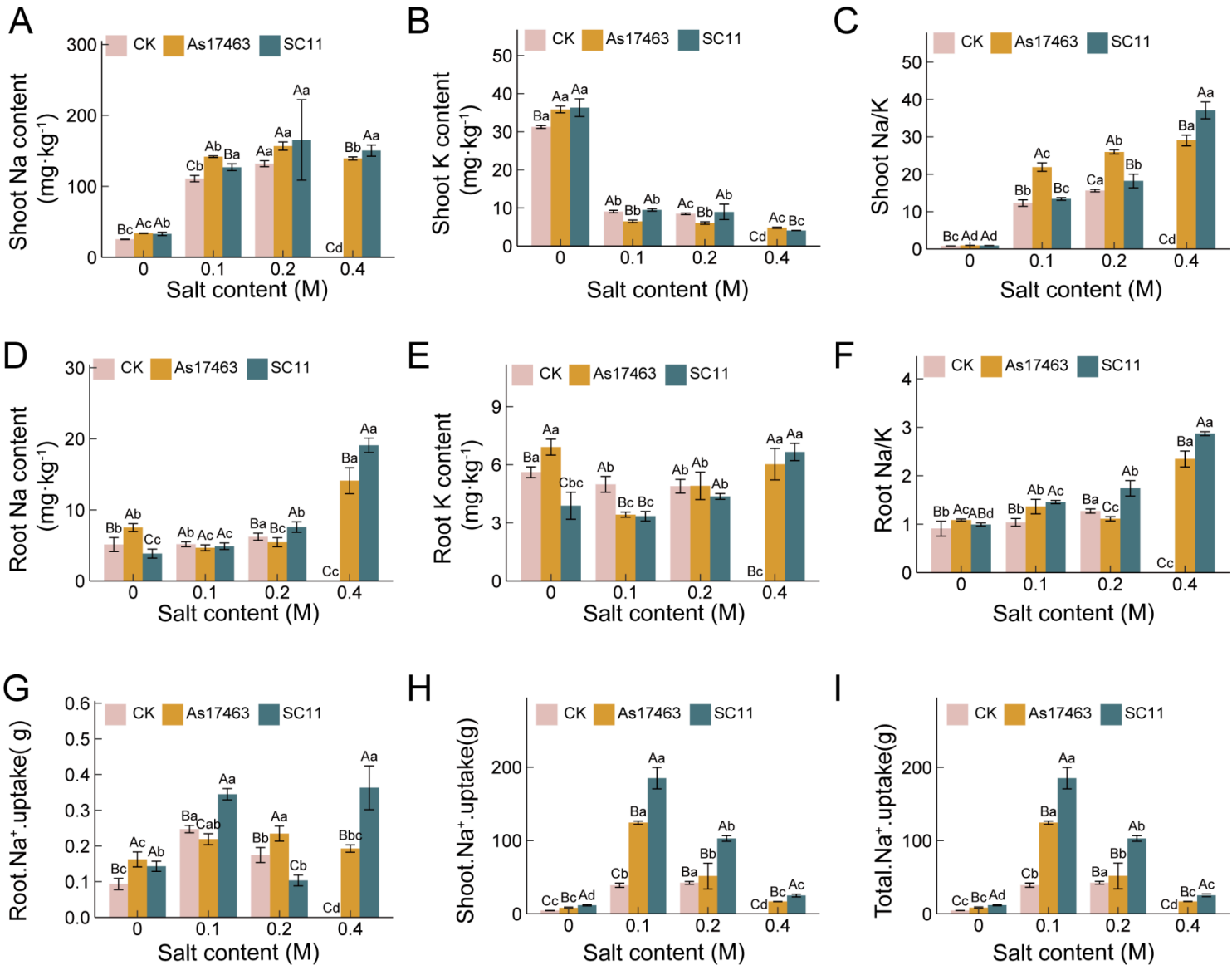

Figure 2

Effects of SC11 and As17463 inoculation on Na^+ and K^+ homeostasis in *S. salsa* under salt stress. (A–C) Na^+ and K^+ concentrations and Na^+/K^+ ratio in shoots. (D–F) Na^+ and K^+ concentrations and Na^+/K^+ ratio in roots. (G–I) Na^+ uptake in roots, shoots, and the whole plant. Data are presented as means ± SE (n = 4). Different uppercase letters indicate statistically significant differences among inoculation treatments at the same salt concentration ($P < 0.05$), while different lowercase letters indicate significant differences across salt concentrations within the same inoculation treatment ($P < 0.05$).

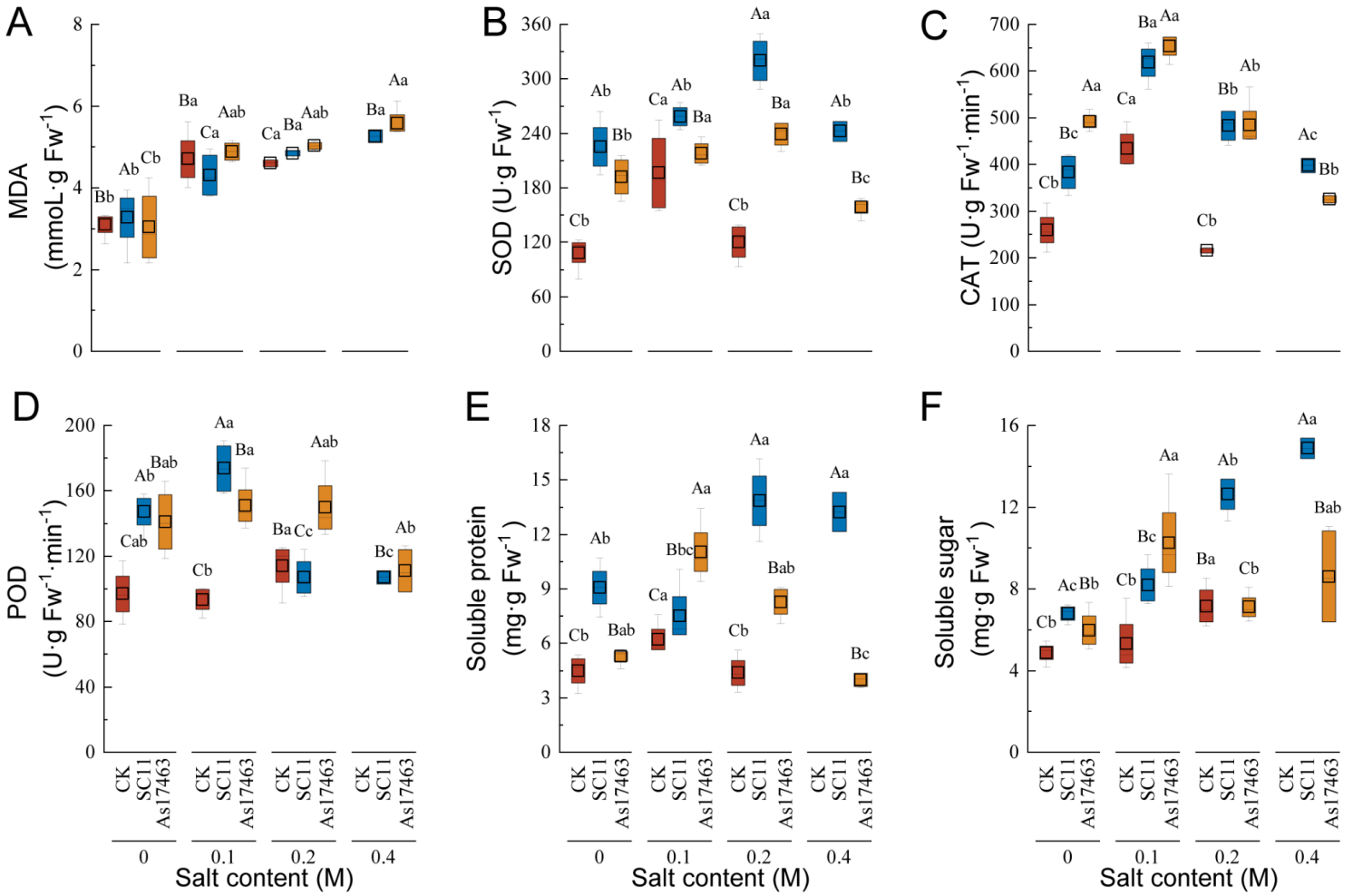

Figure 3

Antioxidant enzyme activities and osmolyte accumulation in *S. salsa* under salt stress following inoculation with different fungal strains. (A) MDA, (B) SOD, (C) CAT, (D) POD, (E) soluble protein, and (F) soluble sugar. Data are presented as means ± SE (n = 4). Different uppercase letters indicate significant differences among inoculation treatments at the same Na_2SO_4 concentration ($P < 0.05$), while different lowercase letters indicate significant differences across salt concentrations within the same inoculation treatment ($P < 0.05$).

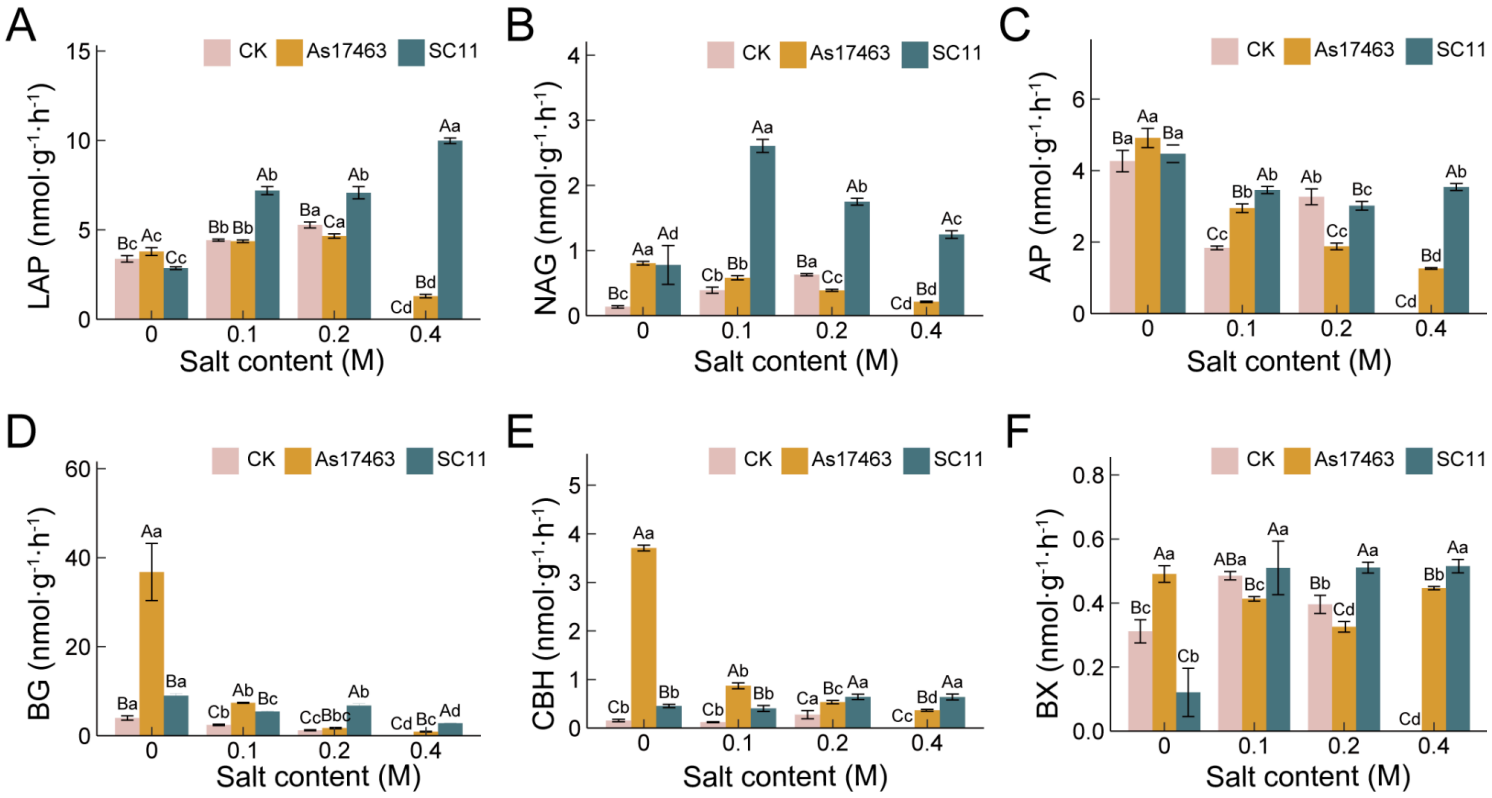

Figure 4

Effects of salt stress and fungal inoculation on rhizosphere soil enzyme activities. Activities of (A) LAP, (B) NAG, (C) AP, (D) BG, (E) CBH, and (F) BX in rhizosphere soils. Data are presented as means ± SE (n = 4). Different letters indicate statistically significant differences ($P < 0.05$). SC11 inoculation maintained or enhanced nitrogen-, phosphorus-, and carbon-degrading enzyme activities under saline conditions.

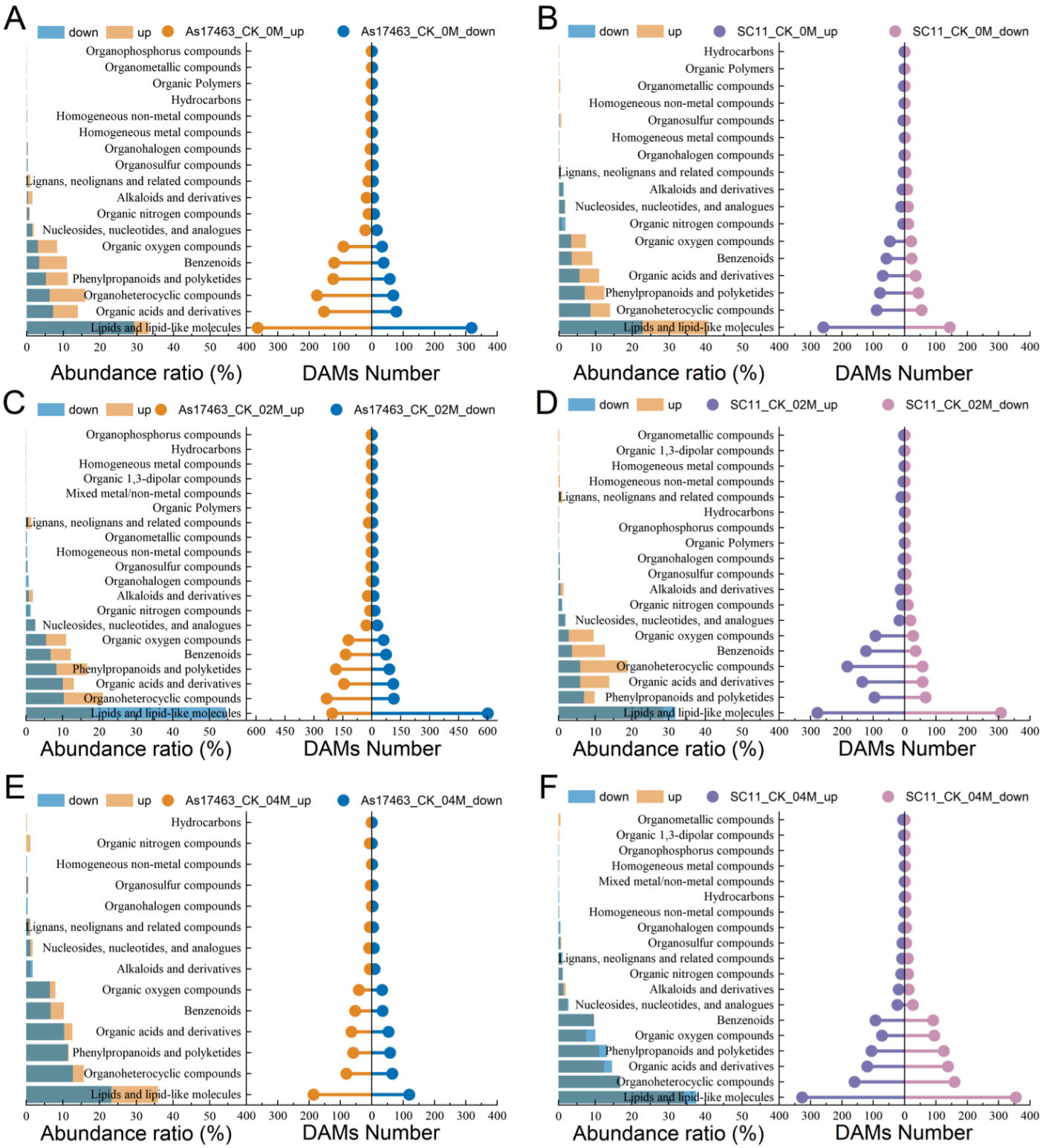

Figure 5

Classification and abundance distribution of DAMs under varying Na_2SO_4 concentrations.

Panels A–F show functional category distribution and abundance ratios of DAMs in pairwise comparisons between CK and the fungal inoculations: As17463 (A, C, E) and SC11 (B, D, F) under 0 M (A, B), 0.2 M (C, D), and 0.4 M (E, F) Na_2SO_4. Left panels indicate the proportion (%) of upregulated (orange)

and downregulated (blue) metabolites within each chemical class. Right panels display the total number of DAMs per category.

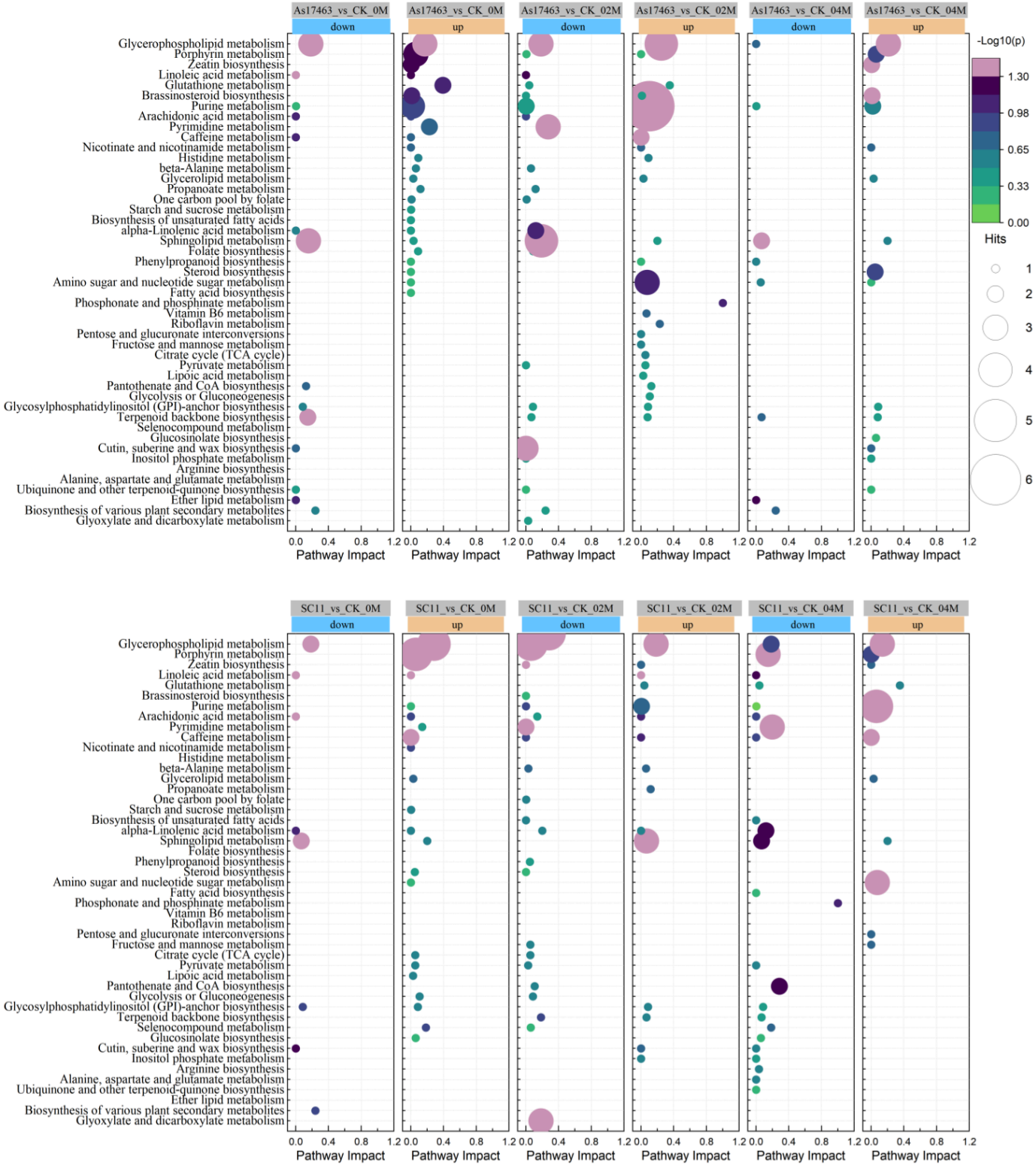

Figure 6

Pathway impact analysis of DAMs under varying Na_2SO_4 concentrations. Bubble plots depict the metabolic pathway impact and significance for upregulated and downregulated DAMs in As17463 vs. CK

(top panels) and SC11 vs. CK (bottom panels) under 0 M, 0.2 M, and 0.4 M Na_2SO_4. Each bubble represents a KEGG pathway; bubble size corresponds to the number of DAMs (hits) mapped to the pathway, and bubble color indicates statistical significance ($-\log_{10}$ p-value). Pathway impact values are plotted on the x-axis, and KEGG pathway names on the y-axis, highlighting the principal metabolic processes modulated by salt stress in each fungal treatment.

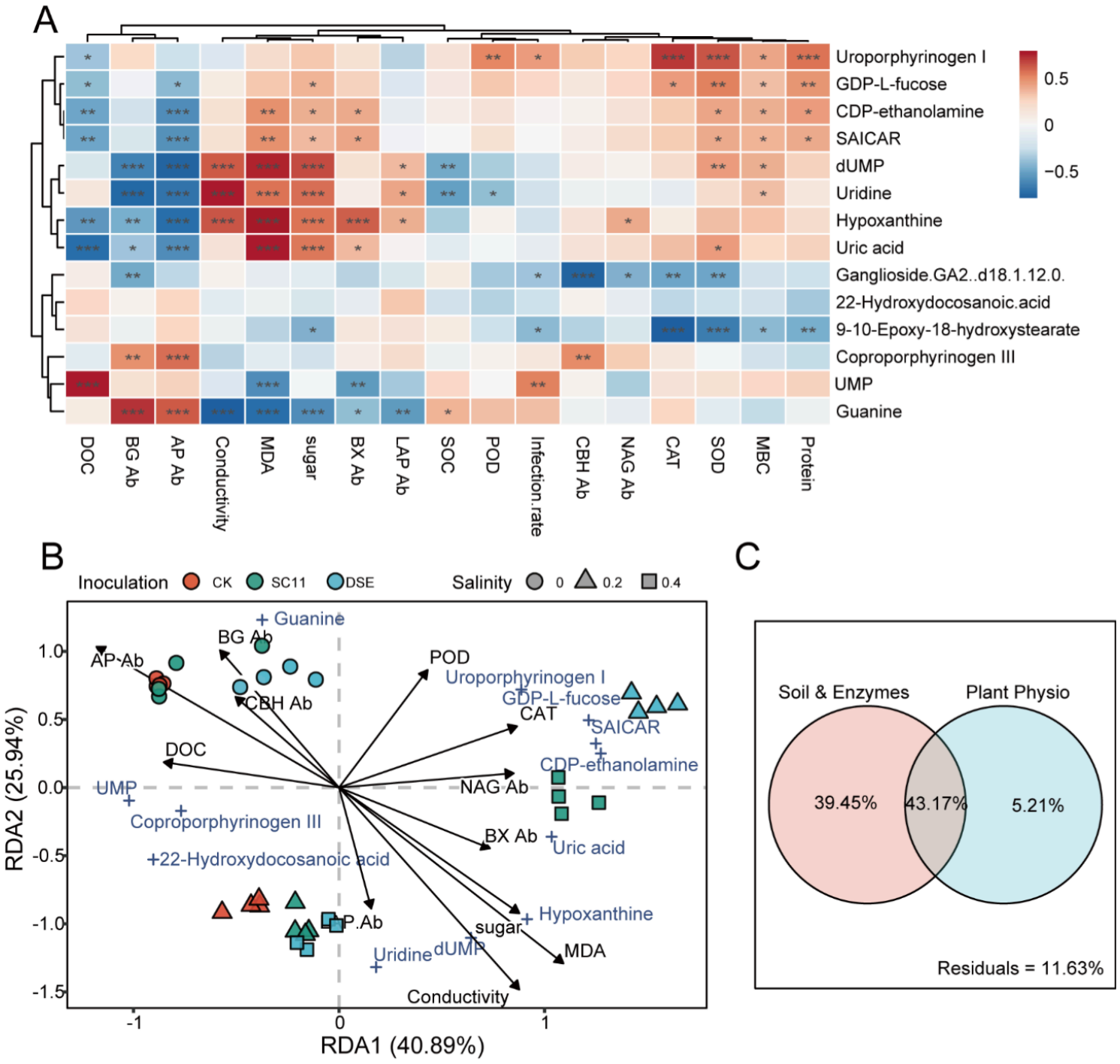

Figure 7

Integrated correlations, ordination, and variance partitioning of metabolites, soil properties, and plant physiological traits under inoculation and salinity gradients. (A) Spearman correlation heatmap

illustrating the relationships between differentially accumulated metabolites (DAMs), soil physicochemical properties, extracellular enzyme activities, and plant physiological indicators. (B) Redundancy analysis (RDA) ordination showing the multivariate responses of metabolomic profiles across inoculation treatments (CK, SC11, and As17463) and salinity gradients (0, 0.2, and 0.4 M Na_2SO_4). (C) Variance partitioning analysis (VPA) quantifying the relative contributions of soil-related variables and plant physiological traits to overall metabolomic variation.

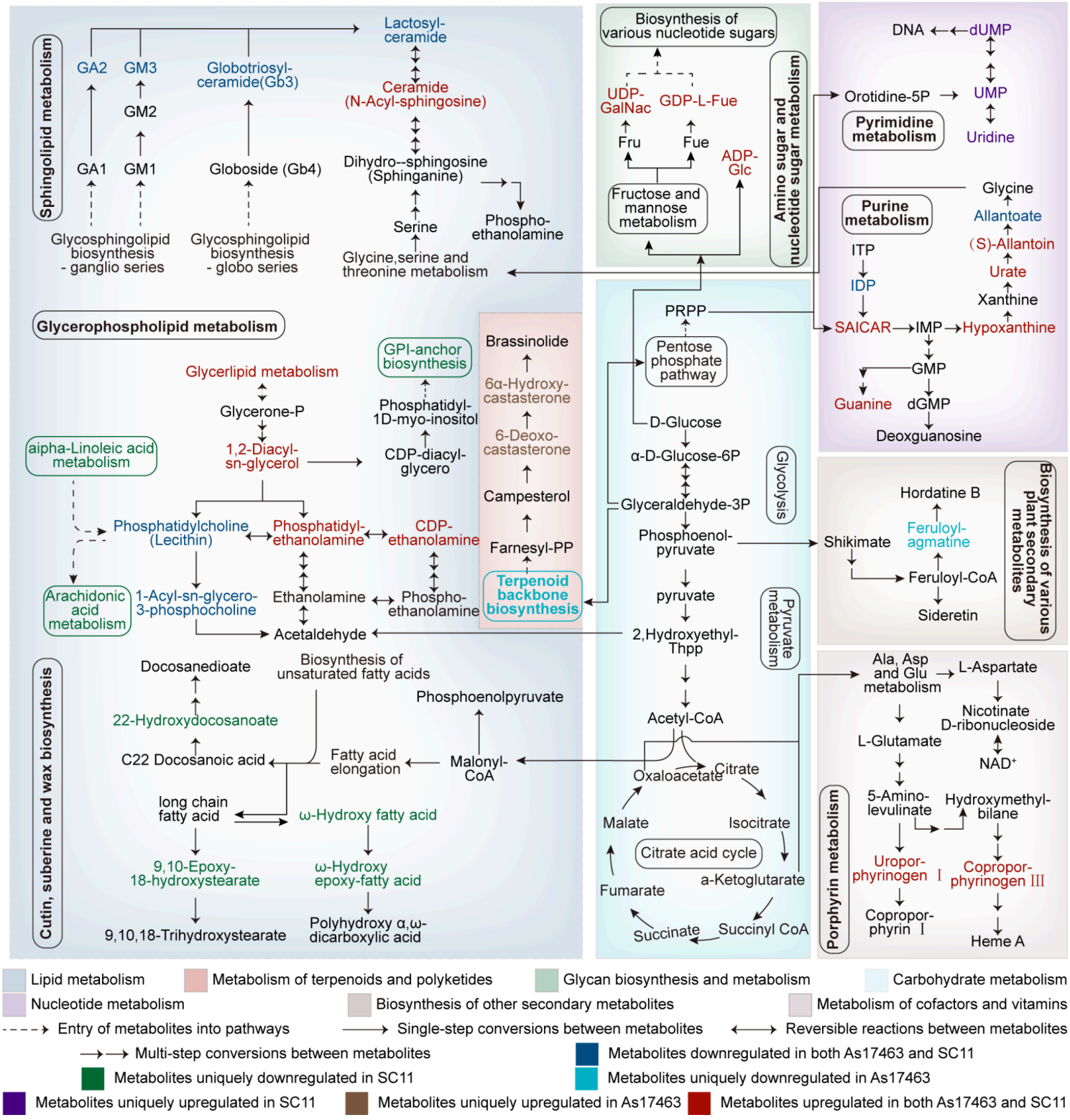

Figure 8

Schematic of DSE strain–mediated enhancement of salt tolerance in *S. salsa* under salt stress.

Supplementary Files

This is a list of supplementary files associated with this preprint. Click to download.

- supplementarymaterials.docx